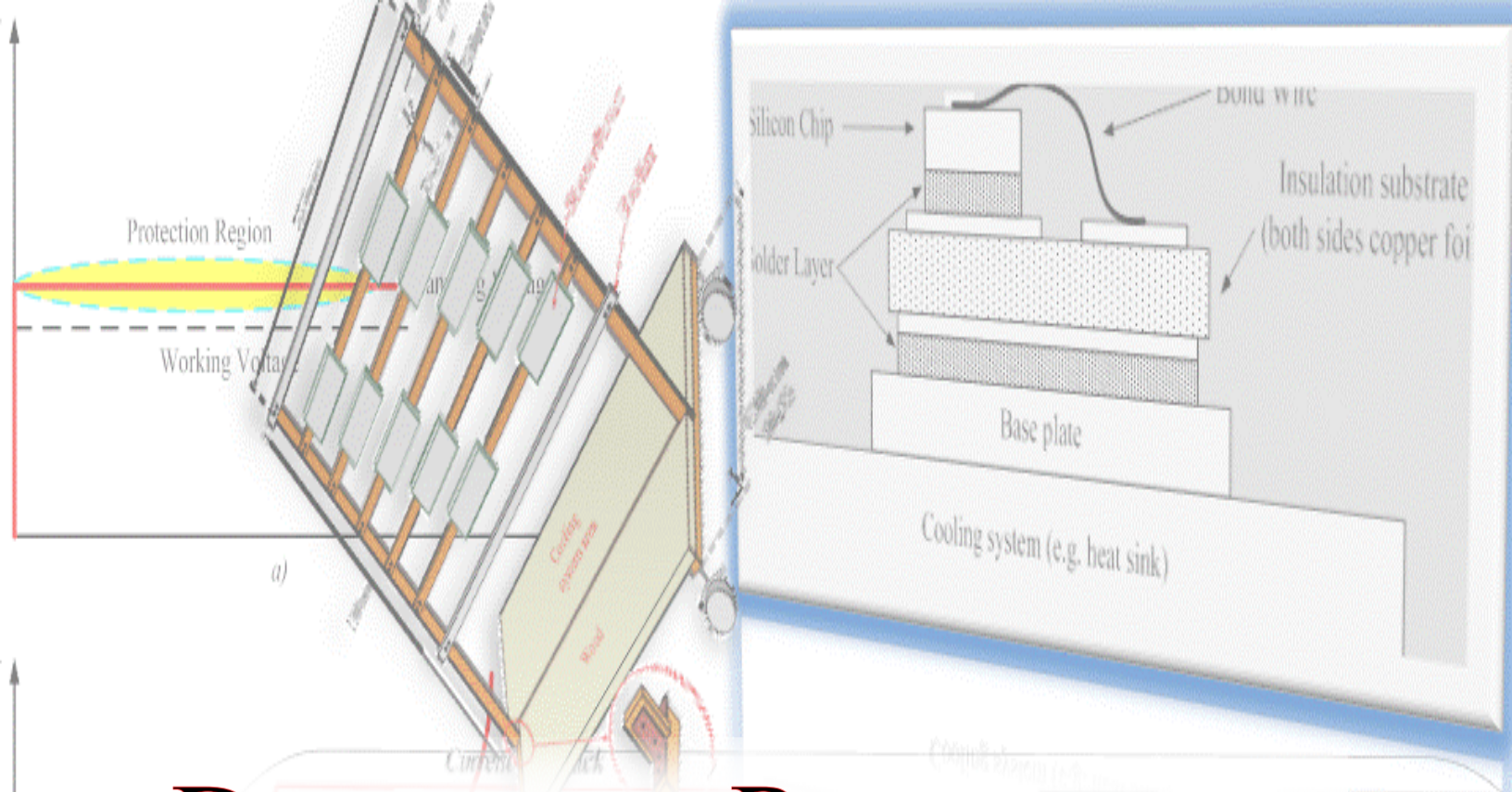

DEVELOP A RELIABILITY TEST SYSTEM FOR IGBT POWER MODULES

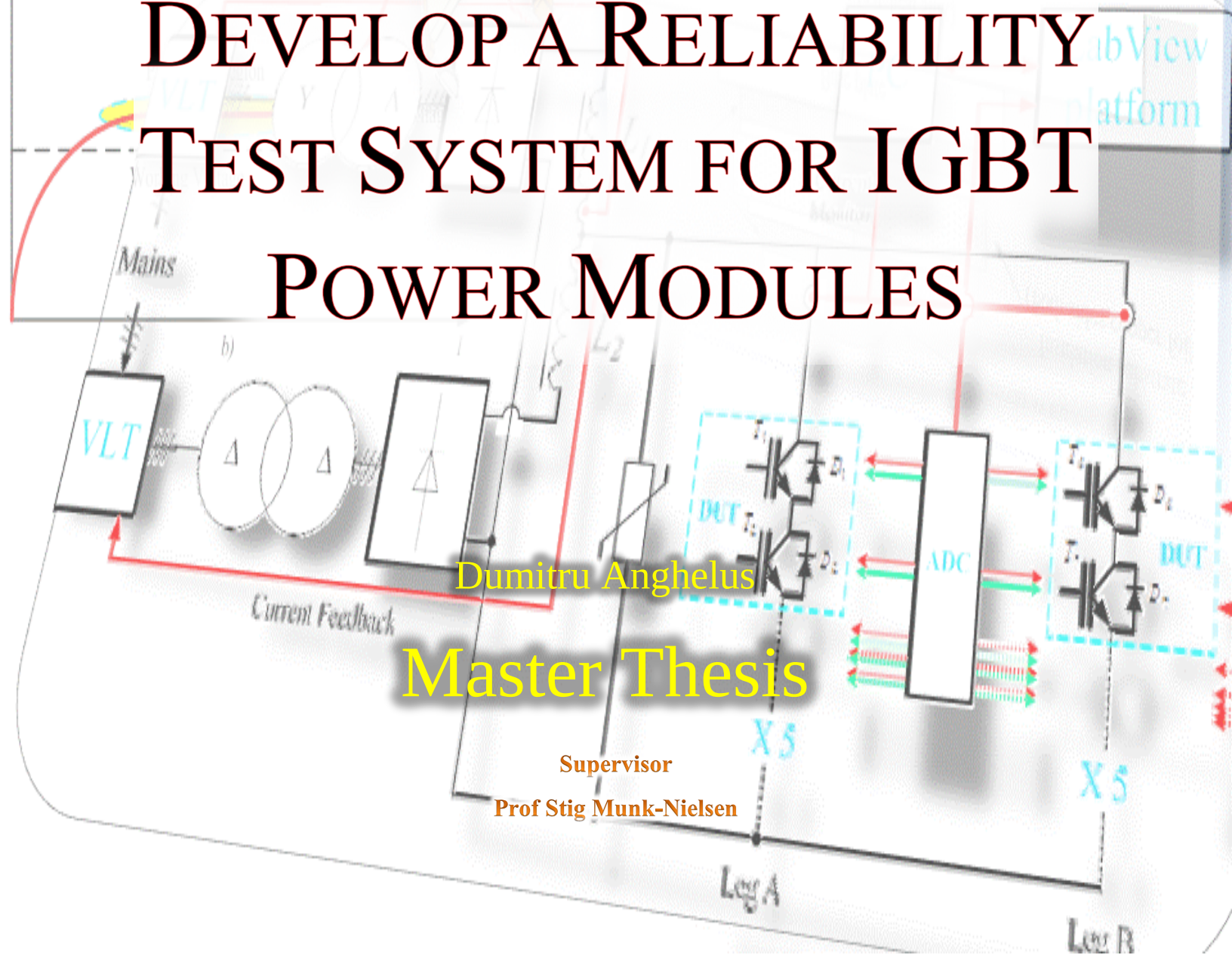

Dumitru Anghelus

Master Thesis

Supervisor

Prof Stig Munk-Nielsen

PREFACE

The wellbeing of the contemporary world's environmental is strongly depended by its efficient performance and its use of electric energy. Power electronics and motor drives have reached every corner of the world from kitchen appliances to high voltage power electronics in wind turbines and still ongoing on an exponential evolution from one year to other.

The presented project approaches in general the reliability issues of IGBT power module used in wind turbines through thermal and power cycling, respectively. Starting from general knowledge and background of the IGBT reliability, all the way through simulation components design and development, the proposed reliability testing system is analyzed in the dedicated chapters.

Almost each page of these earlier mentioned chapters it contains a detailed picture or a colorful block diagram for a better understanding of the proposed testing system. Most of the literature used to write these presented pages were written and draw from the point of view of power electronics industry outline.

One of the outlines withdrawn from the power electronics industry was taken by having a field trip into German industry in Nuremberg at the biggest research community in the world, Fraunhofer.

Special thanks are given to my supervisor, Prof. Stig Munk-Nielsen whose understanding and carefully supervision helped and kept me on the track throughout power electronics field during both semesters.

ABSTRACT

This project is focused on developing a testing system for IGBT power module used in the power electronics unit from the nowadays wind turbines. The dedicated chapters describe after a literally background of IGBT's reliability issues, the proposed testing system within a certain demands and abilities. The main purpose of the system is to be able to do power and thermal cycling of power IGBT module. The proposed system it is mainly summarized from two parts, one electrical and the second is referring to the cooling circuit.

The electrical circuit is analyzed through four different patterns, in order to design it as the best results generating pattern and also the most doable to be immediately implemented in laboratory. The electrical system demands are summed up as a system able to get a current flow of 3000 (A) with a DC-link voltage and current ripple smaller than 5%. The DC-link with the earlier mentioned demands was provided by two power supply sources connected in parallel. The purpose of using two power sources instead of just one, was the idea to use two transformers phase shifted (of 30 degrees) in order to get after rectification a 180 degrees phase shift so the waveforms ripple on the DC-link side could more or less cancel each other by this shiftiness.

The cooling system part was also divided into another two parts; one for cooling the bridge rectifiers and the other for the testing IGBTs. The cooling system for the IGBTs was designed to control the temperature difference (ΔT) on the IGBT surface, in order to enable the ability to test the IGBT power module at different ΔTs within a range of 20-140˚C.

In order to have the cooling circuits close to their components that need to be cooled, two aluminum made chassis were designed and developed for that purpose.

Unfortunately due to some construction and electricity supply delay, the actual IGBT power cycling test couldn't be done and therefore not included in this report, except several voltage measurements of the power supply circuit.

Contents

CHAPTER 1 INTRODUCTION

The intelligent way of using energy is mainly related to goods production, service and maintenance. The advance lifestyle of today's society essentially depends on the wise control of energy. The usable energy is present under several different forms like electrical, mechanical and thermal.

In the wind turbine industry field the reliability issues are on the top list in the Research and Development departments of the companies. The power electronics unit inside every nowadays wind turbine represents the highest failure impact and therefore a very important issue to be addressed.

1.1. Background

The global warming effect has become a very serious matter in the last two decades. In this matter the European Union has demanded the decrease of carbon dioxide emission up to 50% below 1990 levels by the year of 2050 by introducing renewable energy sources [1]. Thereby in 2009 the renewable energy sources provided an average of 18% of the European Union electricity generation with Austria leading with 68%, as Fig. 1.1 shows.

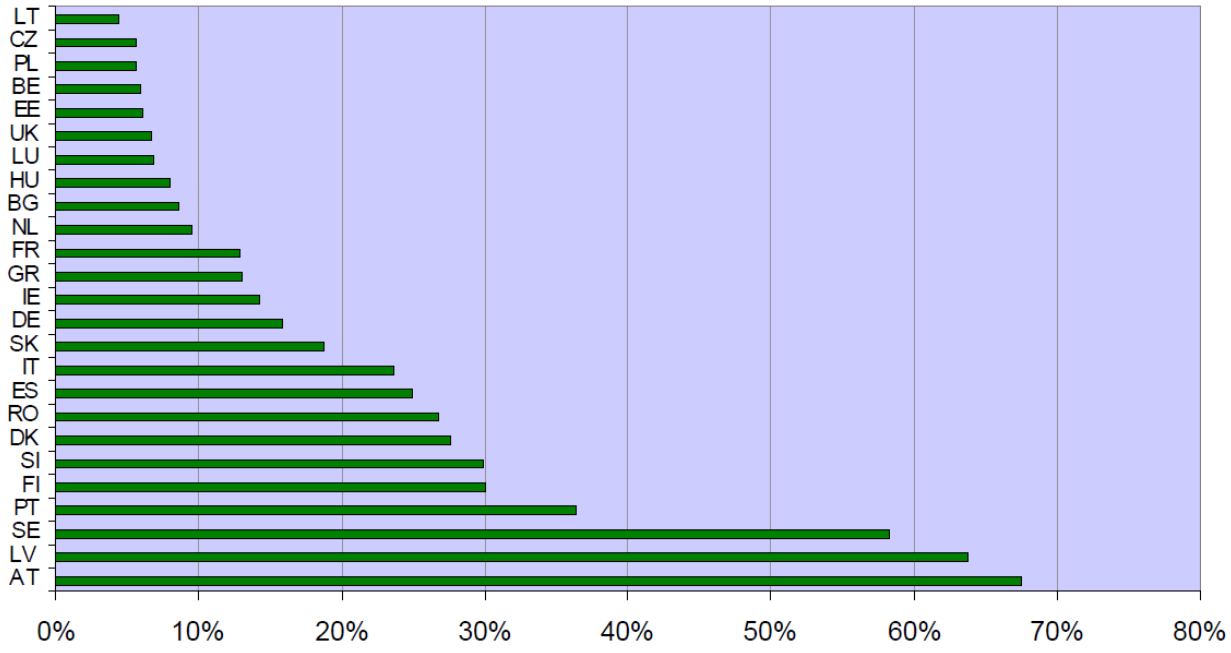

Fig. 1.1. Renewable energy share by country in the European Union by year 2009 [2]

This action demanded by the European Union led to major demands for research, development and reliability of renewable energy sources. Of all renewable energy sources, wind power is currently the most promising natural energy with a positive impact on carbon dioxide

emission reductions, being the most developed power technology in Europe; wind energy installed capacity by December of 2007 was 57 GW in Europe and worldwide 100 GW [1].

During the last three decades the wind turbines have rapidly increased in size demanding a very great deal of power. As the size, structure and ultimately the delivered power were increased, also the failure rates of the wind turbine were increasing. Several studies have been done in the past concerning the failure rate of the wind turbines, and as statistics shows the power converter, whose purpose is to deal with the power delivery to the mains, is one of the major faulty components of the wind turbine. One of the studied cases is represented in Fig. 1.2 downwards.

The frequency converter driven by the stochastic speed of the wind has to generate a fixed frequency, demanded by the grid (e.g. 50Hz). This stochastic profile of the wind has direct influence on the power switching devices of the frequency converter. The temperature of the switching chips is on an ongoing change, stressing the semiconductor devices, especially at low frequencies.

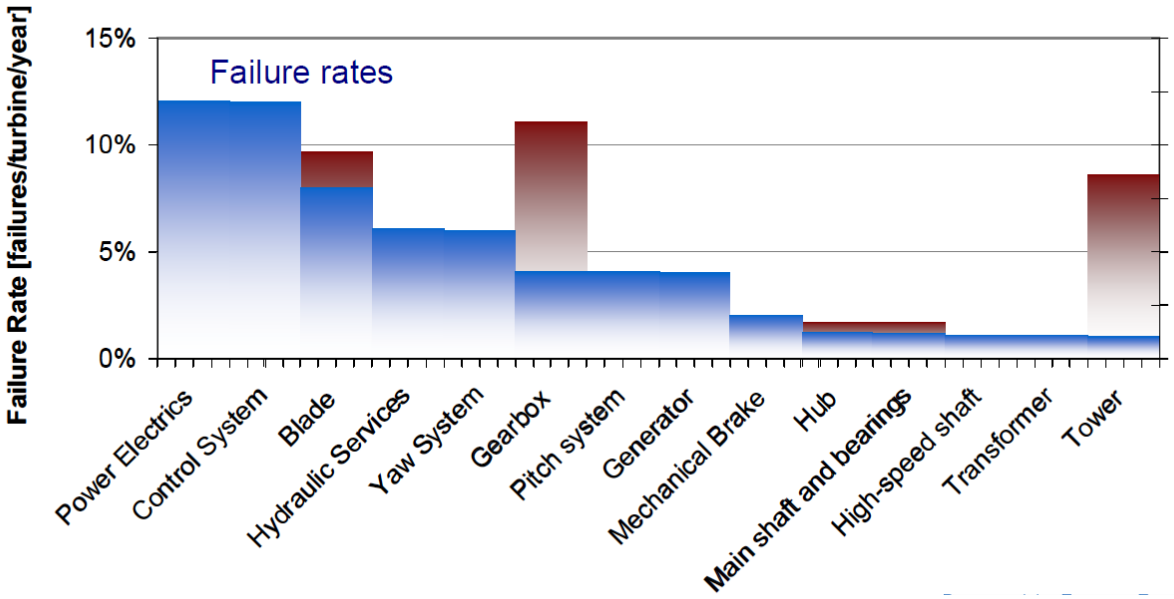

Fig. 1.2. Major failure components rates in a wind turbine [3]

The energy conversion nowadays relies more and more on power switching applications, therefore the manufacturers are demanded to improve the quality and reliability of the switching devices.

Therefore in the following section the properties of the semiconductor switching power devices are analyzed.

1.2. Insulated Gate Bipolar Transistor Overview

The Insulated Gate Bipolar Transistor (IGBT) is the most used semiconductor switching device due to its advantage of lower on-state voltage in comparison with the MOSFET at voltage levels above 800 (V), and low conduction losses in comparison with the Bipolar Transistor. A

sketch from the electrical point of view between the MOSFET and the IGBT is shown in Fig. 1.3.

The one difference between the IGBT and the MOSFET is the added P^+ layer used to inject positive carriers into the *N*-type layer and thereby precipitating conductivity modulation. The structure of the IGBT is presented in Fig. 1.4.

The series-connected *PNPN* junctions form the parasitic thyristor, whose turning-on depends on a critical value of collector current, phenomena known as latch-up. Latch-up is the point where the Gate has no longer control of the collector current, fact that will lead to IGBT destruction.

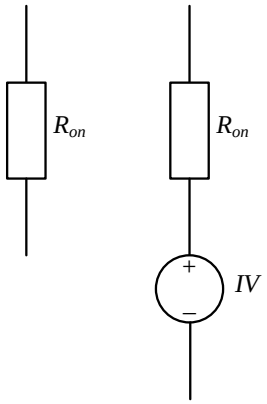

Fig. 1.3. a) MOSFET and b) IGBT sketch from the electrical point of view

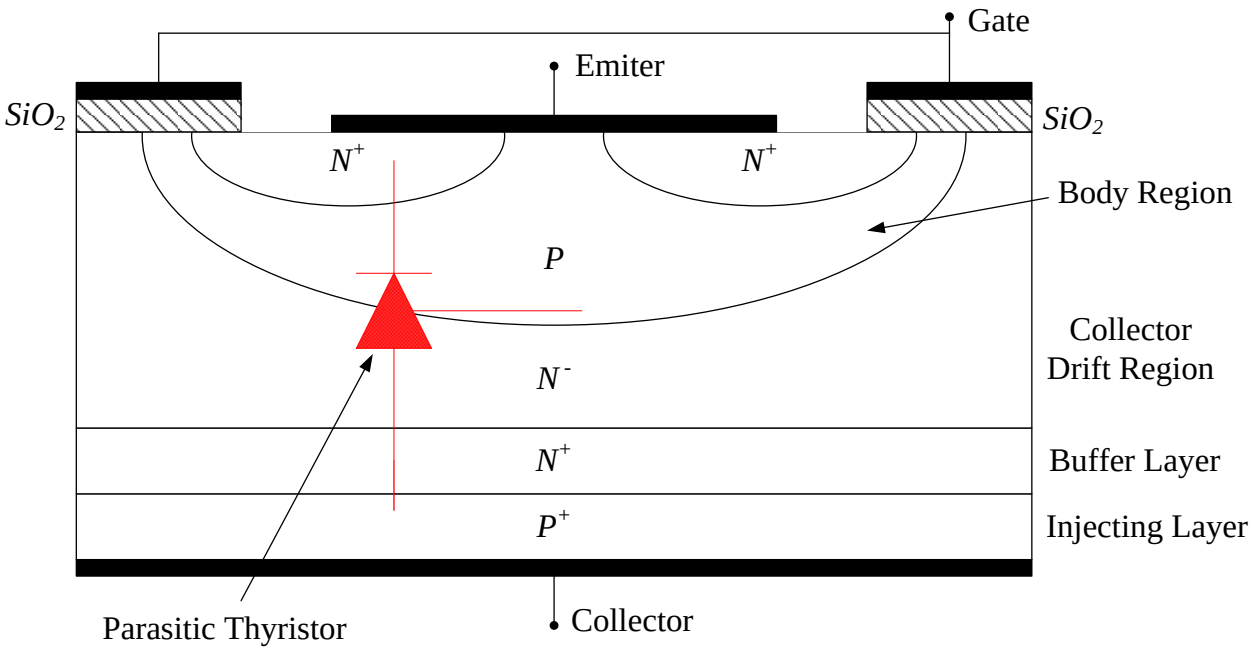

Fig. 1.4. Insulated Gate Bipolar Transistor structure [4]

1.3. Insulated Gate Bipolar Transistor Thermal Model

The switching devices are exposed to different working temperatures depending on the power losses caused by the voltage drop and the current flowing through the device at the same time. The power loss causes the junction temperature to rise and therefore a cooling system is needed to dissipate the heat. This temperature passes through several different layers from the junction to the dissipating point of the cooling system. This process is represented in Fig. 1.5.

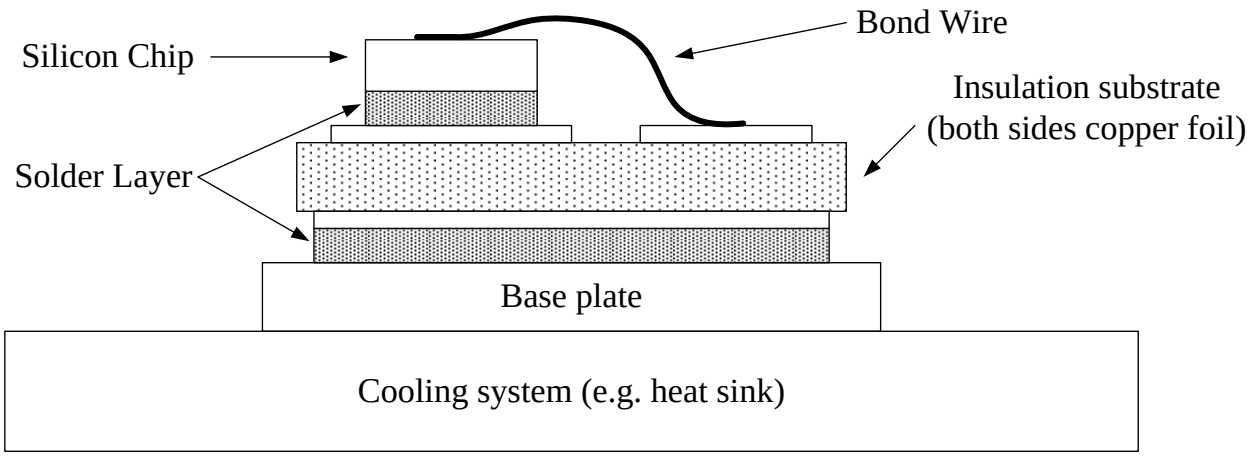

Fig. 1.5. Insulated Gate Bipolar Transistor sectional view [5]

Between each one of these layers there is a thermal resistance and also depending on the materials capability of absorbing an amount of heat there is a so called thermal capacity for each material. Based on these assumptions the equivalent thermal circuit of the IGBT based on the layer structure from Fig. 1.5, is presented in Fig. 1.6.

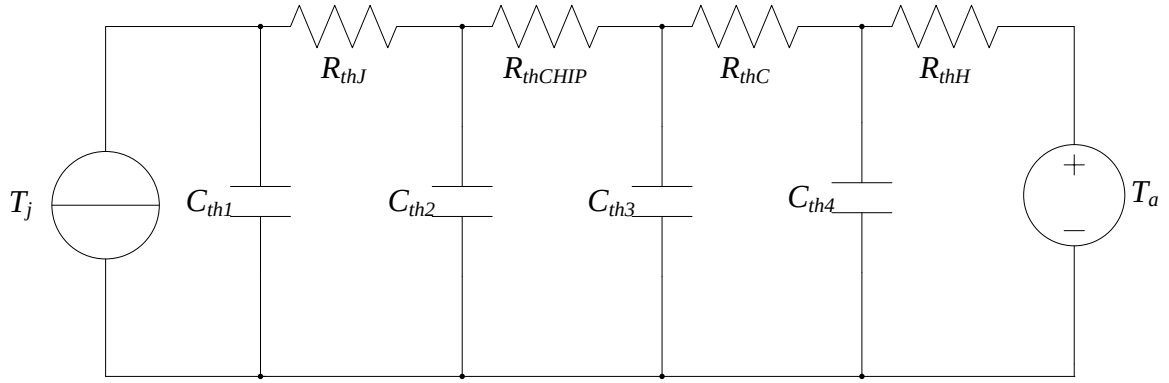

Fig. 1.6. Insulated Gate Bipolar Transistor thermal model equivalent circuit also known as Cauer network

The thermal structure presented in Fig. 1.6 represents the Cauer network. The values of these resistances and capacities for IGBT and for freewheeling diode are given in the datasheet as shown in Fig. 1.7a and b respectively, but for Foster thermal network. A simple conversion from Foster to Cauer network can be done using Plecs.

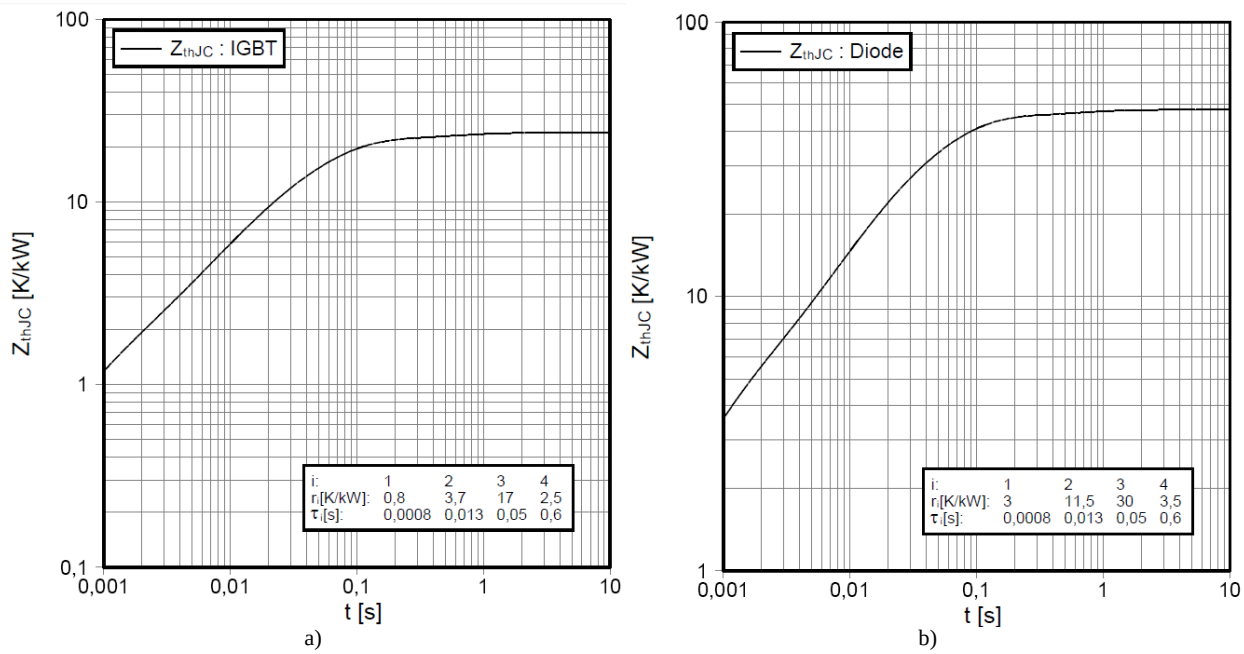

Fig. 1.7. a) IGBT thermal impedance, and b) Diode thermal impedance, data for Foster network [6]

1.4. Reliability of IGBT Power Module

The nowadays semiconductor companies face two important issues in terms of leading success of their products, and that is the quality as well the reliability of their products. The reliability of a power module depends on the structure of the components, their semiconductor material properties and on interferences with internal and external stresses.

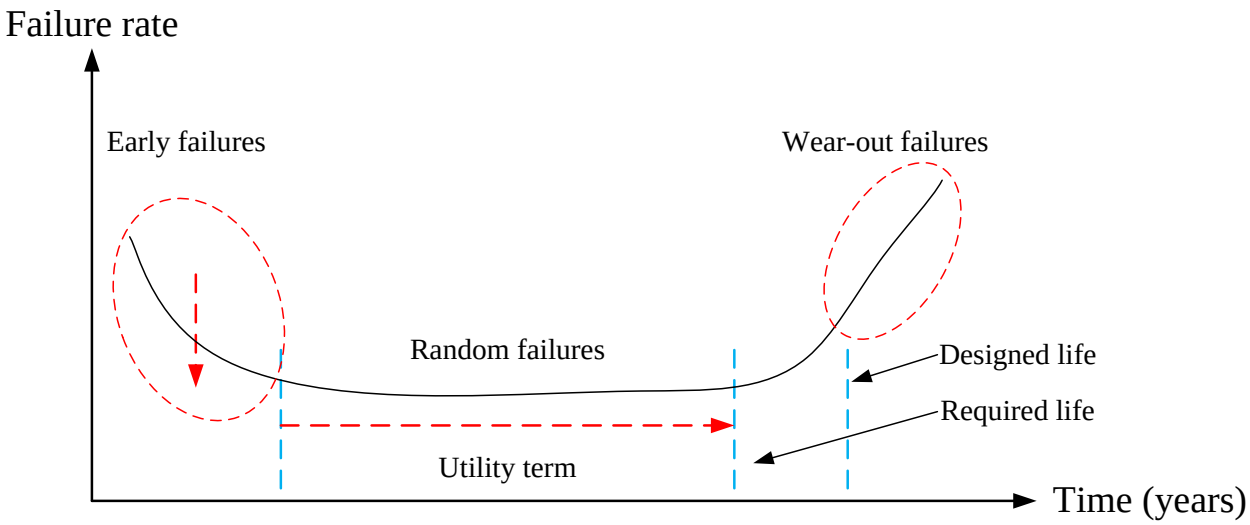

Fig. 1.8. Bathtub curve – Change in failure rate as a function of time [7]

In the last decade the improvements of semiconductor technology of the power modules has rapidly increased alongside with their reliability. Basically the reliability of a product inquires the understanding of failure mechanism and determination of failure rate.

The failure rate of electronics parts and equipment in time is represented by the so called bathtub curve containing three types of failures, as shown in Fig. 1.8.

Considering IGBT power modules, early failures can be defined as human errors like touch the gate and emitter wires, cracking in Direct Copper Bonded (DCB) layer, bad design, etc. Random failures are generated by external accidents or stresses like overcurrent, overvoltage, particle radiation and so on. And finally the wear-out failures are defined as accumulation of incremental physical damage or fatigue during normal load operation, and therefore very difficult to control.

Among other factors, thermal fatigue failure is one of the factors deciding the lifetime of a power module. The thermal fatigue appears between the chip and the bond wire or between the isolation layer and the copper base plate, causing the thermal resistance or the on-resistance to increase beyond the specified value from datasheet [8].

1.4.1. Power Cycle Curve

The thermal stress applied to the IGBT power modules due to temperature swing up and down will subject the internal structure of the IGBT to mechanical stress what will lead to mechanical fatigue, deterioration and finally a breakdown. This process has direct negative influence on the lifetime of the IGBTs. This temperature swing or temperature cycle is called "power cycle life" and it can be predicted using the power cycle curve which is the curve of the number of cycle as a function of temperature swing.

An example is given in Fig. 1.9 where is represented the commanded pulse of the tested IGBT and the measured temperatures, during one cycle.

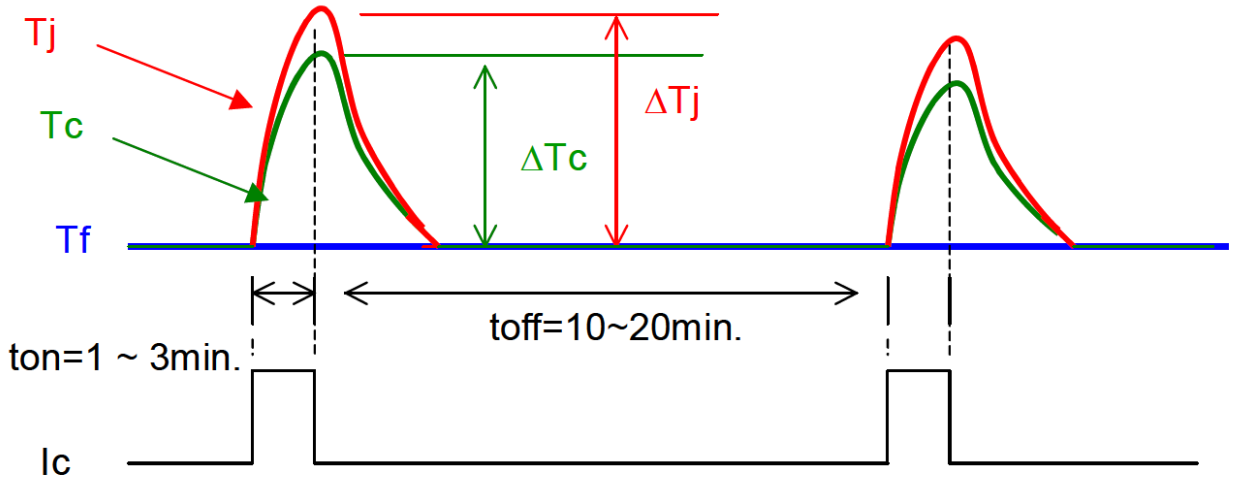

Fig. 1.9. Junction (ΔT_j) and case (ΔT_c) temperature variation during one cycle, an example [7]

There are two types of power cycle curves depending on the monitoring temperature from which will result two different points of failure or cracking within the IGBT power module.

One curve is represented as a function of junction temperature swing (ΔT_j) as shown in Fig. 1.10a. The failure caused by this type of test appears as a crack at the interface between the silicon chip and the bond wire, as shown in Fig. 1.11a. And the other power cycle curve also known as thermal cycle is represented as a function of case temperature swing (ΔT_c), with a predominant failure caused by deterioration of the soldered area between the DCB insolation layer and the base plate, as shown in Fig. 1.10b and 1.11b, respectively.

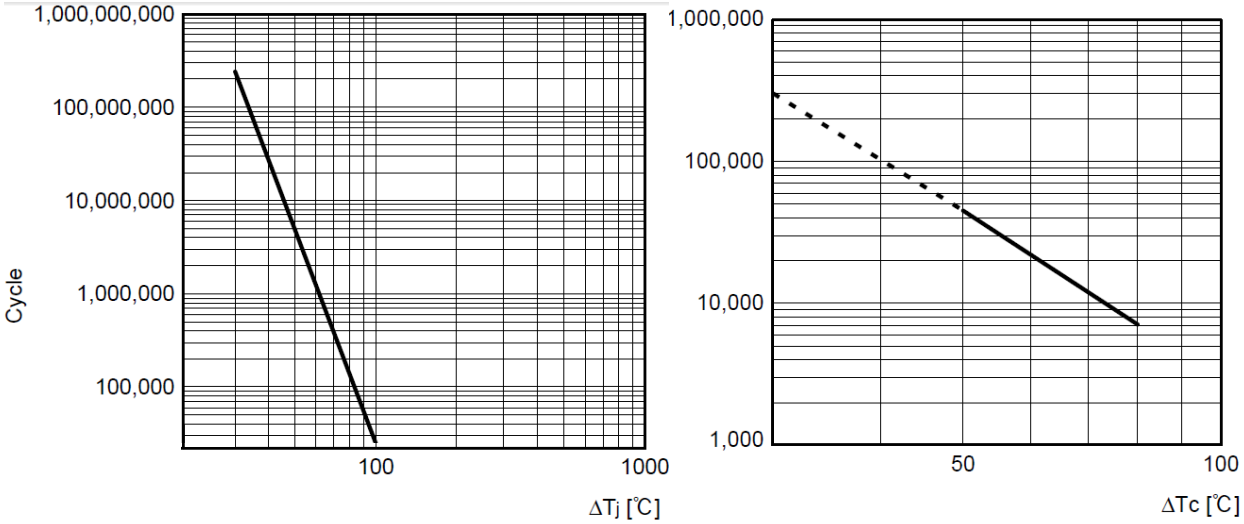

a) b)

Fig. 1.10. a) ΔT_j and b) ΔT_c power cycle life until failure [5]

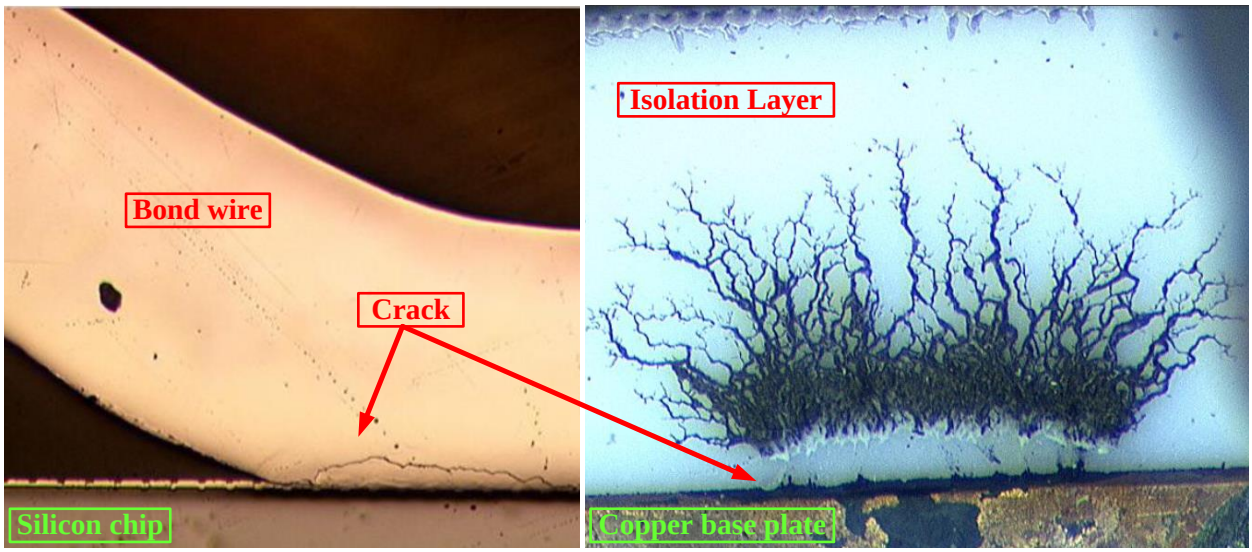

a) b)

Fig. 1.11. a) Failure between the silicon chip and the bond wire due to junction temperature variation, and b) Failure between the isolation layer (DCB) and the copper base plate due to case temperature variation [9]

The power cycle life of an IGBT power module can be calculated as proceeded in the example showed in Eq. (1.1). If for example the power cycle of a certain test is 1500 kilocycles and the length of one cycle is 15 minutes, then the lifetime of the tested module is:

$$\frac{1500 \cdot 10^3 \cdot 15}{60 \cdot 24 \cdot 365} = 42.8 \approx 42\ (years) \tag{1.1}$$

1.5. Objective of the Work

1.5.1. Problem Description

The industry of power modules has been widely covering many various applications like renewable energy conversion, electric vehicle and so on. The market of power modules has demanded all sorts of new and more reliable properties for various applications and as the market growth it is expected to extend their properties and functionality [8].

The reliability of power modules has been pointed up between the most important matters on the industry market reports [5]. On the market of wind industry, especially offshore wind applications where the power electronic units are inaccessible, the reliability issues are of great concern. Therefore the reliability of power electronics is on the high priority list in R&D departments.

To be able to get applicable results, characteristics of power modules and their behavior, an investigation through different stress tests has to be done.

1.5.2. Project Solution

The objective of this project thesis is to build a testing system capable for generation of ware out of several modules lifetime of IGBT power modules used in wind turbines power electronics unit. The system has to be able to test IGBT devices at their rated current under different temperature stress conditions.

Basically the system will be used to power cycle life and predict the lifetime under different temperature variation. For keeping the tested device at a certain constant temperature a cooling system has to be designed and build alongside the electric circuit of the system.

Therefore the following chapter will present the system description and modeling, both the electrical and cooling circuit. In chapter 3 the control and circuit analysis are presented and analyzed. Chapter 4 is presenting the measurements of the designed testing system, and finally in chapter 5 are drawn the conclusions.

The actual experimental results are put under limitation for this report due to some construction and electricity delay in the laboratory.

CHAPTER 2 SYSTEM DESCRIPTION

Scientific modeling represents an essential part of all scientific activity either if is mathematically, graphically or conceptual. Therefore this chapter the proposed testing system is analyzed and all its contents like electrical and cooling item are designed through simulation whereas is necessary.

2.1. System Overview

As stated in the previous chapter, last section, a system capable of delivering a wide range of knowledge about IGBT power module has to be designed and build. The proposed system it is described in a detailed manner in the following section, and its main purpose is to investigate the power and thermal cycle, respectively, of the IGBT power modules under different temperature variations (ΔT).

In order to generate a wide range of different knowledge about IGBTs, the system was designed in a flexible manner from the point of view of its capability to investigate different tasks or goals for that manner. For this purpose many months were spent on its design, in order to add up more different testing capabilities to its final outline.

Going down to our testing procedure, the system was designed to generate knowledge about power cycling and thermal cycling. For this manner the system was set under a standard 30 seconds pulses testing process, in order to stress the IGBTs on both the chip layer and the insulation layer (DCB layer), at the same time and at different temperature variations.

The testing system has been proposed by Vestas to test the IGBT power modules under stresses equivalent as possible as they are stressed in the industry fields. Therefore in table 1 the demands that the testing system has to meet are specified.

Table 1. IGBT POWER MODULES TESTING SYSTEM SPECIFICATIONS

Parameter	***Ratings***
DC current	Up to 3000 (A)
Testing time	1-30 (s) ON and 1-30 (s) OFF
DC Voltage/Current ripple	Maximum 5%
Test temperature variations (ΔT)	From 30˚ to 140˚

Therefore in the next section, part by part the electrical and the cooling circuits of system are described in a detailed manner.

2.2. System Description

2.2.1. Electrical Circuit

On this section the electrical components and the connections and interactions between each other are defined and designed. Therefore the next section it is presenting the electrical diagram of the system together with its simulation in order to generate knowledge about the rated values of the components.

The electrical diagram of the system is presented in Fig. 2.1 downwards. The working principle of the circuit it is very simple as it can be seen in the figure, two powerful supply sources are connected in parallel in order to rich the demand of 3000 (A) on the DC link side, whereas two sets/legs of 5 IGBTs/DUTs (Drive Under Test) are connected in parallel. The DUTs are designed 5 by 5 in parallel in order to save time. So, when the leg A is ON for 30 (s) the other leg is OFF and likewise when leg B is on.

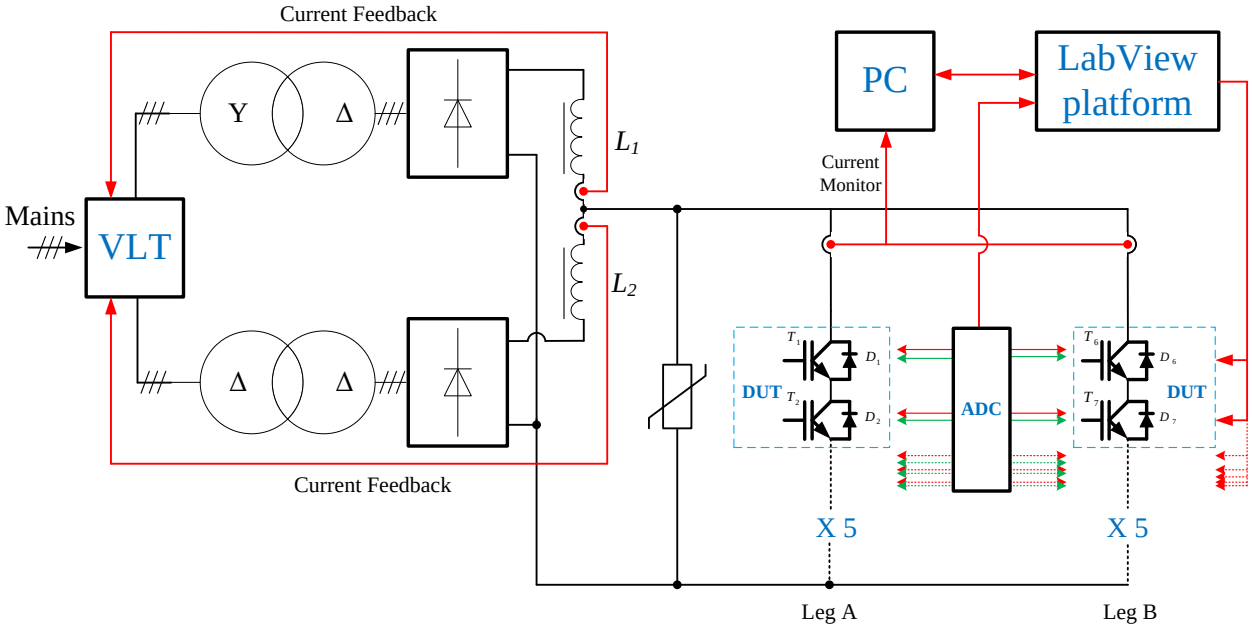

Fig. 2.1. Electrical circuit diagram of the IGBT lifetime (power/thermal cycle) testing system using one VLT for the power supply source

Based on the electrical diagram from Fig. 2.1, a simulation was implemented in LTSpice to adjust and design the electrical components of the system, presented in the forwards section.

2.2.1.1. Simulation

The simulation is presented the same as the electrical system was presented previously, starting from the mains; left side from Fig. 2.1; simulation also showed as LTSpice schematic in annex 2.

First the probability of performing with one VLT and paralleling the transformers on the power supply side was taking in consideration.

Forwards the transformers together with the bridge rectifier are the first components to be simulated and design. Therefore on Fig. 2.2 the current through the YΔ-supplied rectifier is presented. The current on the ΔΔ-supplied rectifier it is not shown because it looks the same, only phase shifted. Design discussed and detailed further on section 2.2.1.4 of this chapter.

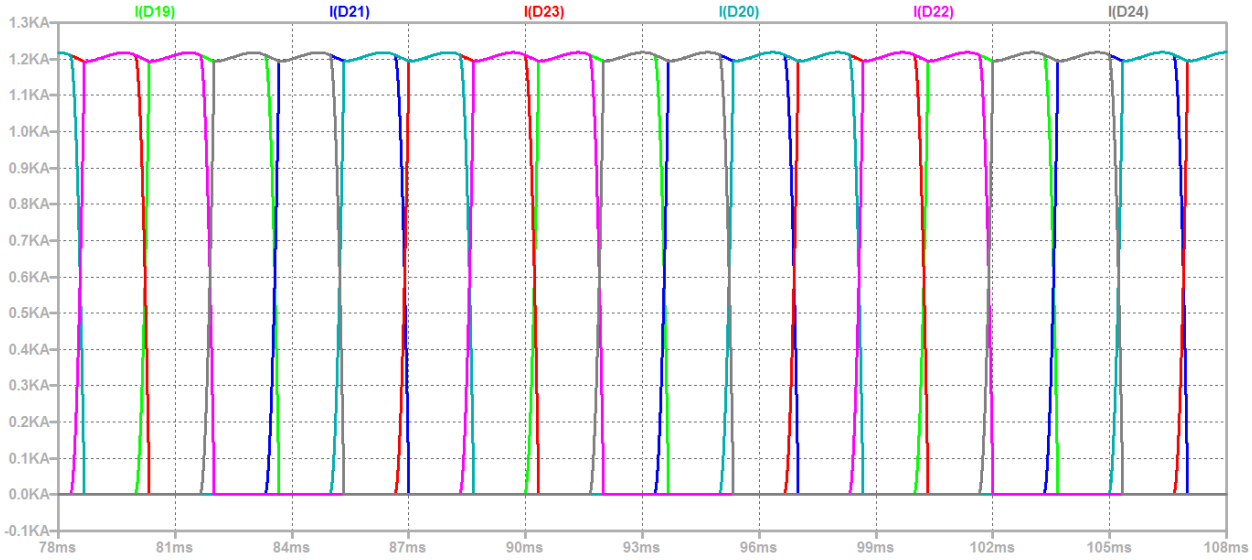

Fig. 2.2. The current through the YΔ-supplied rectifier diodes at full load of 1200 (A)

In this figure (2.2) the current ripple it is shown to be a little higher, problem that it is addressed latter on and shown in the following.

Further on the current through the inductors is presented to shown how the current ripple it is more or less cancel on inductor's output and so on the testing side of the system. This can be seen in Fig. 2.3 illustrated downwards.

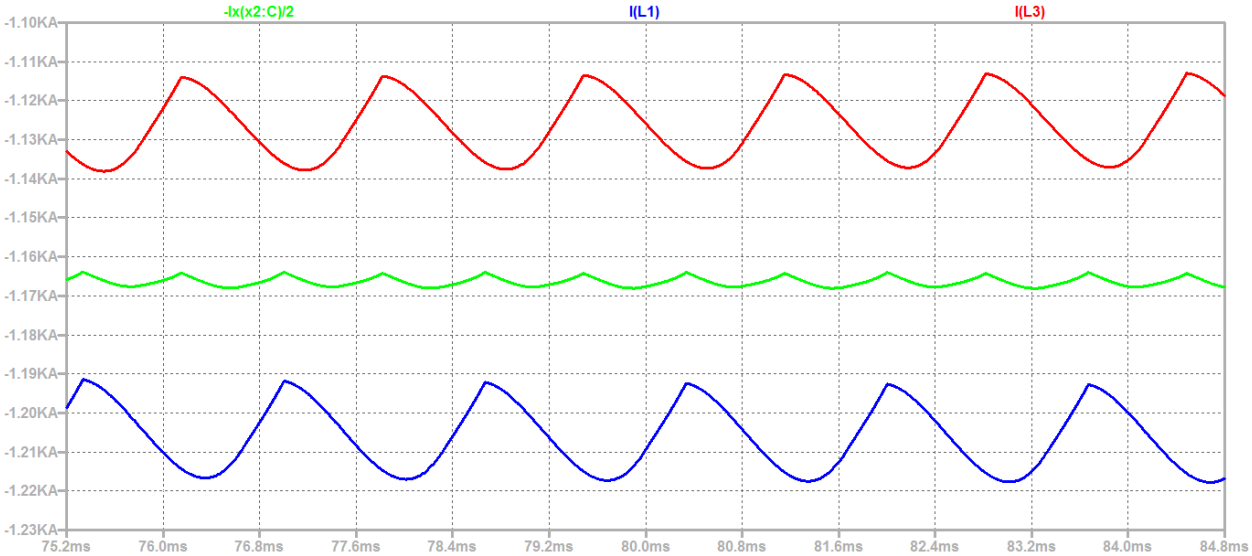

Fig. 2.3. The current ripple through the inductors (blue/top and red/bottom) and the resulted (green/middle) current after paralleling, divided by 2

Due to their different input connections in the figure can be also seen that one transformer is drawing more current than the other.

Due to equivalency only one homemade IGBT based on its datasheet, was implemented for simulations.

Further on the simulation on the testing side is presented in the following figures. First the current and the voltage drop on the DUT (drive under test) turned on at 50 (ms), are shown in Fig. 2.4.

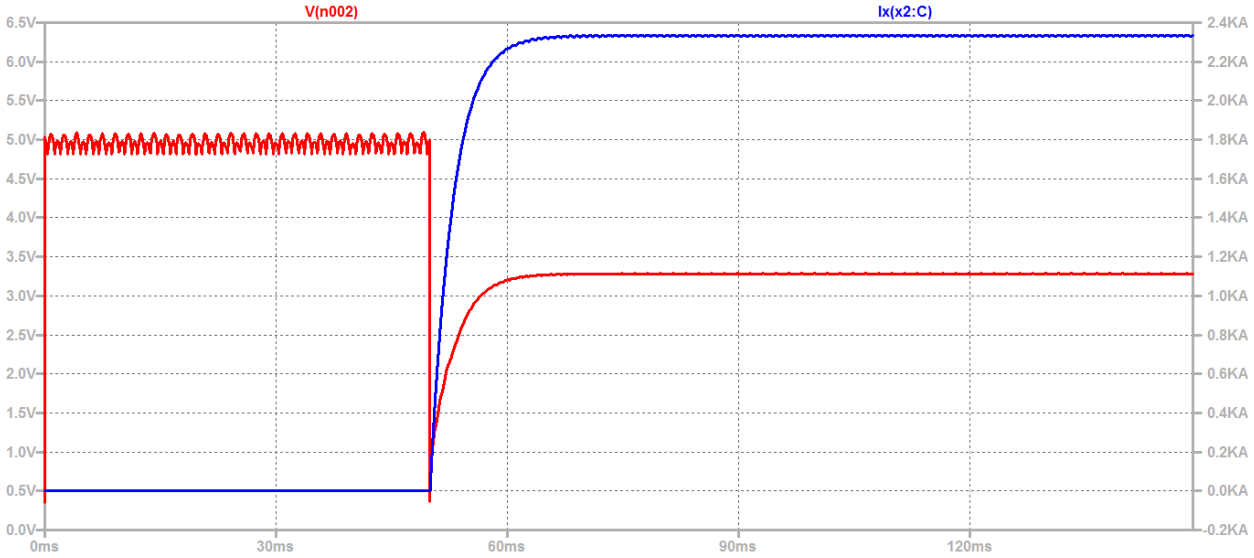

Fig. 2.4. The current on the right scale, and the voltage drop on the left scale, through the testing IGBT (DUT) with a turn-on delay of 50 (ms)

On the next figure, Fig. 2.5 the voltage and current waveforms ripple are presented to ensure that the DC-link ripple is smaller than 5%.

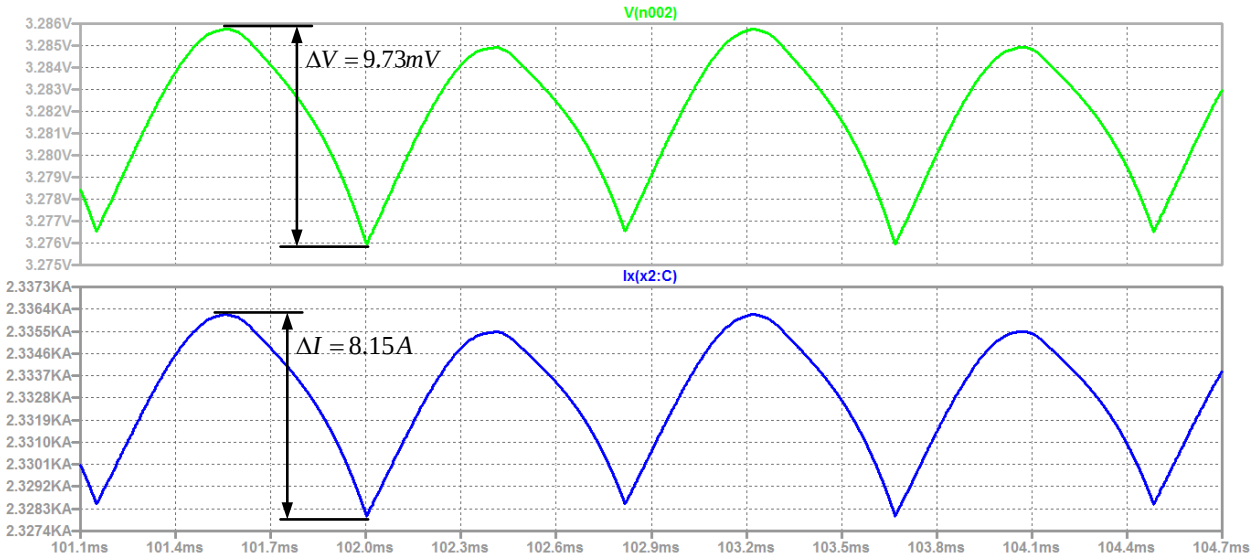

Fig. 2.5. Voltage, on top, and current waveforms ripple on the testing IGBT (DUT)

In the following the voltage drop calculation is analyzed. Recalling from the demands section, the maximum accepted voltage drop it is 5%. This 5% are withdrawn from the following formula:

$$\Delta V = \frac{9.73 \cdot 10^{-3}}{3.2} = 0.003 \leq 5\% \quad (2.1)$$

$$\Delta I = \frac{8.15}{2300} = 0.0035 \leq 5\% \quad (2.2)$$

Based on the presented simulation the electrical components of the system were designed as follows further on the next section.

For the detailed description, the system has been departed in two parts and described separately in the following two sections. Furthermore on the next section the left side of the system or the power supply side it is described.

2.2.1.2. Power Supply Side Description

Fig. 2.6. Picture of the Danfoss VLT frequency converter used for power supply

As it can be seen in Fig. 2.1 the power supply side is composed by the following:

- Danfoss VLT frequency converter;
- High power transformer;
- Bridge rectifier;
- Inductor.

Starting from the left side, the Danfoss made VLT frequency converters are used. The VLT frequency converters used in this project are the VLTs FC-302P55k with the rated power of 55 (kW) at 400 (V). A picture of one of those VLTs is presented in Fig. 2.6.

In order not to stress to much the transformers the output of the VLT was filtered using an Danfoss ordered three-phase LC-filter of 115 (A) as its rated current. A picture of it is shown in Fig. 2.7.

Fig. 2.7. 115 (A) three-phase LC-filter used between the VLT and the transformers

The high power transformers were custom designed analytically by hand and afterwards the details were sent to the manufacturer. In the following it is presented the calculation of the transformer. For starts the parameters known are shown in table 2. The electrical circuit for this design is presented in Fig. 2.8 downwards.

Table 2. KNOWN PARAMETERS FOR TRANSFORMER DESIGN

Parameter	***Symbol***	***Value***
Efficiency	η	0.9
Power Factor	$cos\ \varphi$	0.6
Output Voltage	V_{out}	20 (V)
Output Current	I_d	1500 (A)
Line-line Primary Voltage	V_{ll}	400 (V)
Maximum Power of the Transformer	P_{max}	35 (kW)

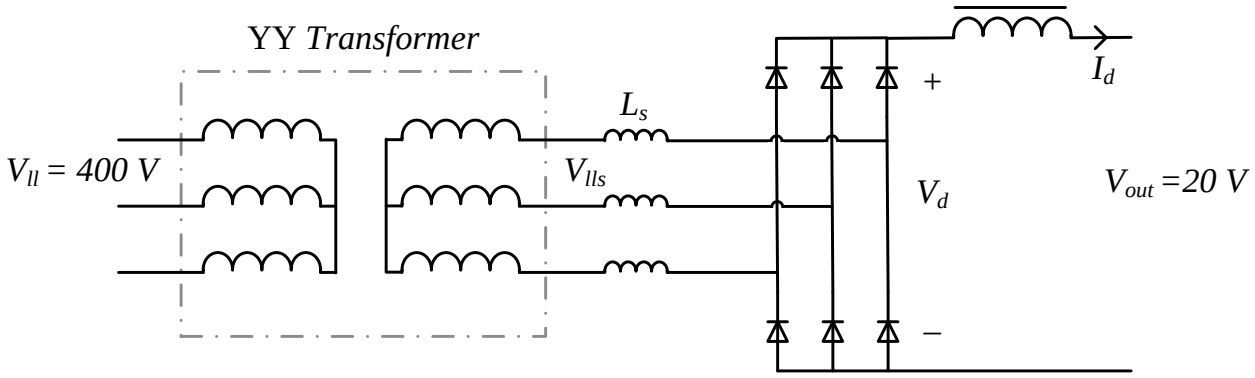

Fig. 2.8. Electrical circuit for designing the transformer

With the known parameters from table 2 the line-to-line secondary voltage (V_{lls}) of the transformer could be calculated as:

$$V_d = \frac{3\cdot\sqrt{2}}{\pi}\cdot V_{lls} - \frac{3\cdot\omega\cdot L_s}{\pi}\cdot I_d \tag{2.3}$$

From Eq. (2.3) the needed voltage is extracted considering that $I_d = 0$ as written in Eq. (2.4-2.5).

$$V_{lls} = \left(V_d + \frac{3\cdot\omega\cdot L_s}{\pi}\cdot I_d\right)\cdot\frac{\pi}{3\cdot\sqrt{2}} \tag{2.4}$$

$$V_{lls} = 25\cdot\frac{\pi}{3\cdot\sqrt{2}} = 19\ (V_{rms}) \tag{2.5}$$

Now by knowing the output voltage (V_d) and current (I_d) needed on the DC-link side, the maximum active power of the transformer can be calculated, and from there the total apparent power of the transformer will results, as written in the following two equations:

$$P_{max} = P_{dc} = I_d\cdot V_d = 1500\cdot 20 = 30\ (kW) \tag{2.6}$$

$$S = \frac{P_{dc}}{\eta} \cdot \frac{1}{\cos\varphi} = \frac{30000}{0.9} \cdot \frac{1}{0.6} = 55\ (kVA) \tag{2.7}$$

Furthermore knowing the apparent power and the line-line voltage on the primary side, the line-line current (I_{ll}) and the impedance (Z_{base}) of the primary side of the transformer can be calculated as follows in Eq. (2.8) and (2.9).

$$I_{ll} = \frac{S}{V_{ll}} = \frac{55000}{400} = 137.5\ (A) \tag{2.8}$$

$$Z_{base} = \frac{V_{ll}}{I_{ll}} = \frac{400}{137.5} = 2.9\ (\Omega) \tag{2.9}$$

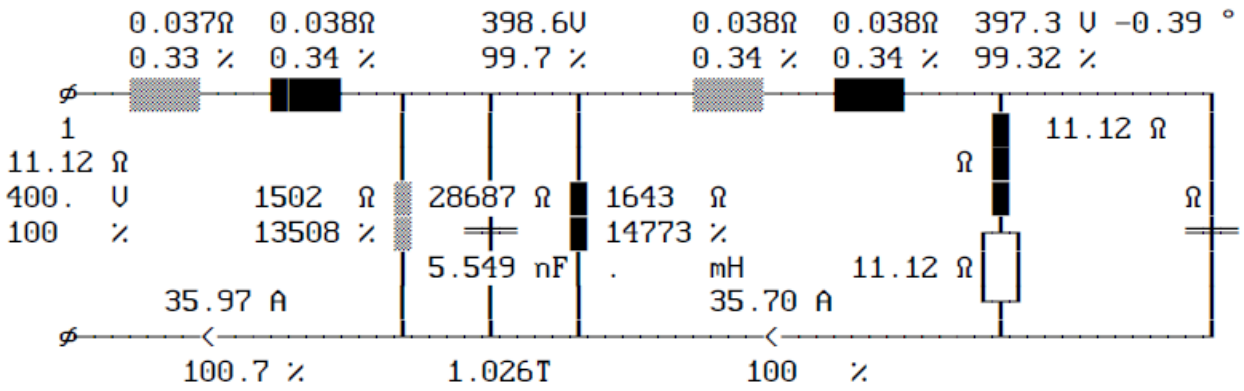

a)

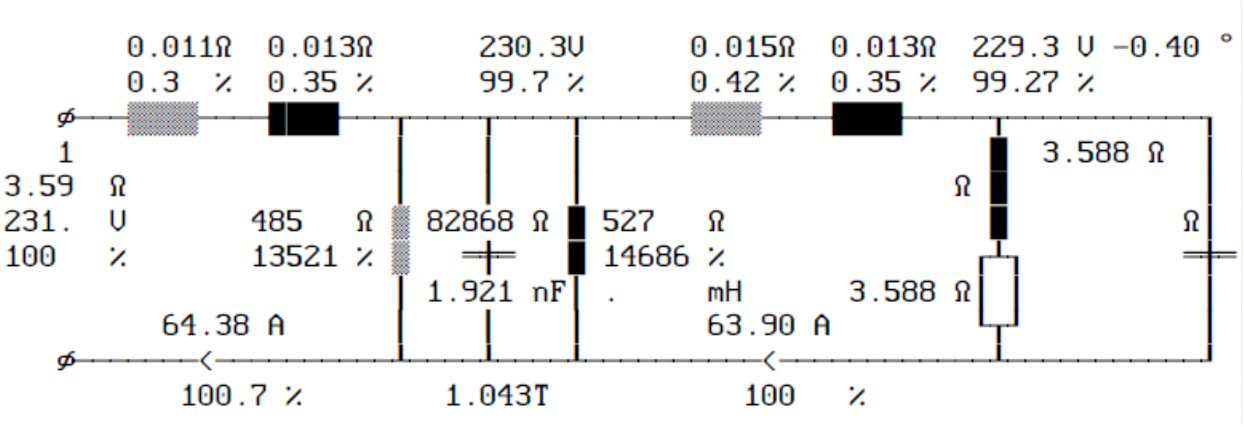

b)

Fig. 2.9. Technical datasheet of the a) ΔΔ-Transformer and b) YΔ-Transformer from the manufacturer

And at the last the leakage inductance for both the primary (L_p) and the secondary (L_s) sides respectively, are calculated in the following two equations as:

$$L_p = \frac{0.04 \cdot Z_{base}}{2 \cdot \pi \cdot 50} = \frac{0.04 \cdot 2.9}{2 \cdot \pi \cdot 50} = 0.37\ (mH) \tag{2.10}$$

$$L_s = \frac{L_p}{\left(\frac{n_p}{n_s}\right)^2} = \frac{0.37 \cdot 10^{-3}}{\left(\frac{400}{19}\right)^2} = 0.83\ (\mu H) \tag{2.11}$$

This analytic handmade design of the transformer was just approximately figures for the manufacturer. According to this the equivalent circuits of both of the transformers provided from the manufacturer are shown in Fig. 2.9. Because their maximum power was only 35 (kVA), the electrical system was then designed using two power supplies in parallel, in order to reach the demanded output power of 3000 (A) and 20 (V).

Fig. 2.10. Picture of the transformers used for power supply the 3000 (A) DC-link

The second very important demand in designing the output power was that the maximum voltage ripple on the DC-link side should be not higher than 5%. So, this ended up to be a very big problem knowing that a 1 (F) capacitor bank could hardly solve the DC-link voltage ripple.

Furthermore several simulations have been run and the solution for decreasing the DC-link voltage ripple has turned out to be simpler than using a 1 (F) capacitor bank. The solution was to use two different transformers from the point of view of their connections. So, one of those were designed as ΔΔ-Transformer and a YΔ-Transformer, option that was leading to a 30˚ phase shift on the output of the transformers, so 180˚ after rectification, and therefore on the DC-link side the voltage ripple of one transformer it is 180˚ out of phase of the other. This shiftiness lead to a DC-link voltage ripple smaller than 0.5% because the actual voltage ripple of one transformer was more or less canceling the voltage ripple of the other. A picture of the transformers it is presented downwards in Fig. 2.10.

The parameters of the both transformers are written down in table 3.

Table 3. TRANSFORMERS PARAMETERS FROM MANUFACTURER DATASHEET

Transformer type	*Parameter*	*Value*
YΔ	Rated frequency	100 (Hz)
	Turns ($^{n_p}/_{n_s}$)	$^{46}/_{4}$
	Efficiency	0.98
	Voltage ($^{input}/_{output}$)	$^{231}/_{25}$ (V)
	Current ($^{input}/_{output}$)	$^{64}/_{1557}$ (A)
ΔΔ	Rated frequency	100 (Hz)
	Turns ($^{n_p}/_{n_s}$)	$^{81}/_{4}$
	Efficiency	0.98
	Voltage ($^{input}/_{output}$)	$^{400}/_{25}$ (V)
	Current ($^{input}/_{output}$)	$^{36}/_{1531}$ (A)

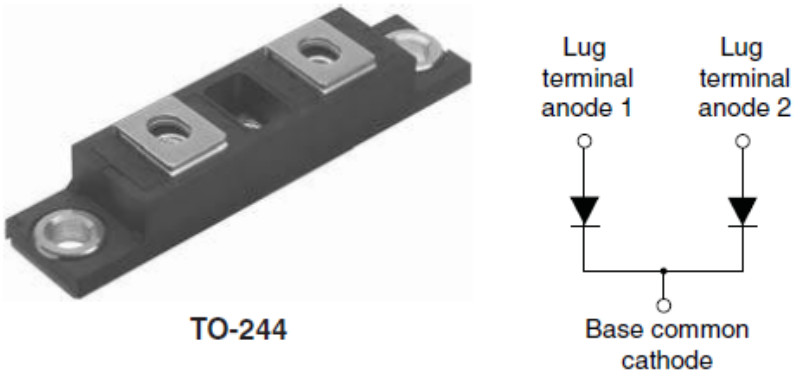

Fig. 2.11. Picture and inside connection of the schottky diodes used for rectification [10]

After the transformer's design the diodes design were a very difficult one to be made, because the voltage drop across them will have a very big impact on the DC-link side due to the high current. For this project the schottky diodes were the best solution to withstand high current at low voltage and therefore low voltage drop.

From the simulation, presented on the previous sections, the ratings for the diodes were extracted and a 400 (A) with a voltage drop less than 1 (V) was needed. On the market the schottky diodes shown in Fig. 2.11 were found to be available.

This diode is a common cathode connection of two legs/diodes with 200 (A) as their rated current. So, the final bridge rectifier was formed by 12 Schottky diodes connected two by two in parallel so the 400 (A) diode could be formed for each of the 6 devices of the bridge rectifier as shown in Fig. 2.8. Due to the rated current of the selected diodes the total current on the DC side or the testing current was reduces to 2400 (A) instead of 3000 like there was listed in system's demands.

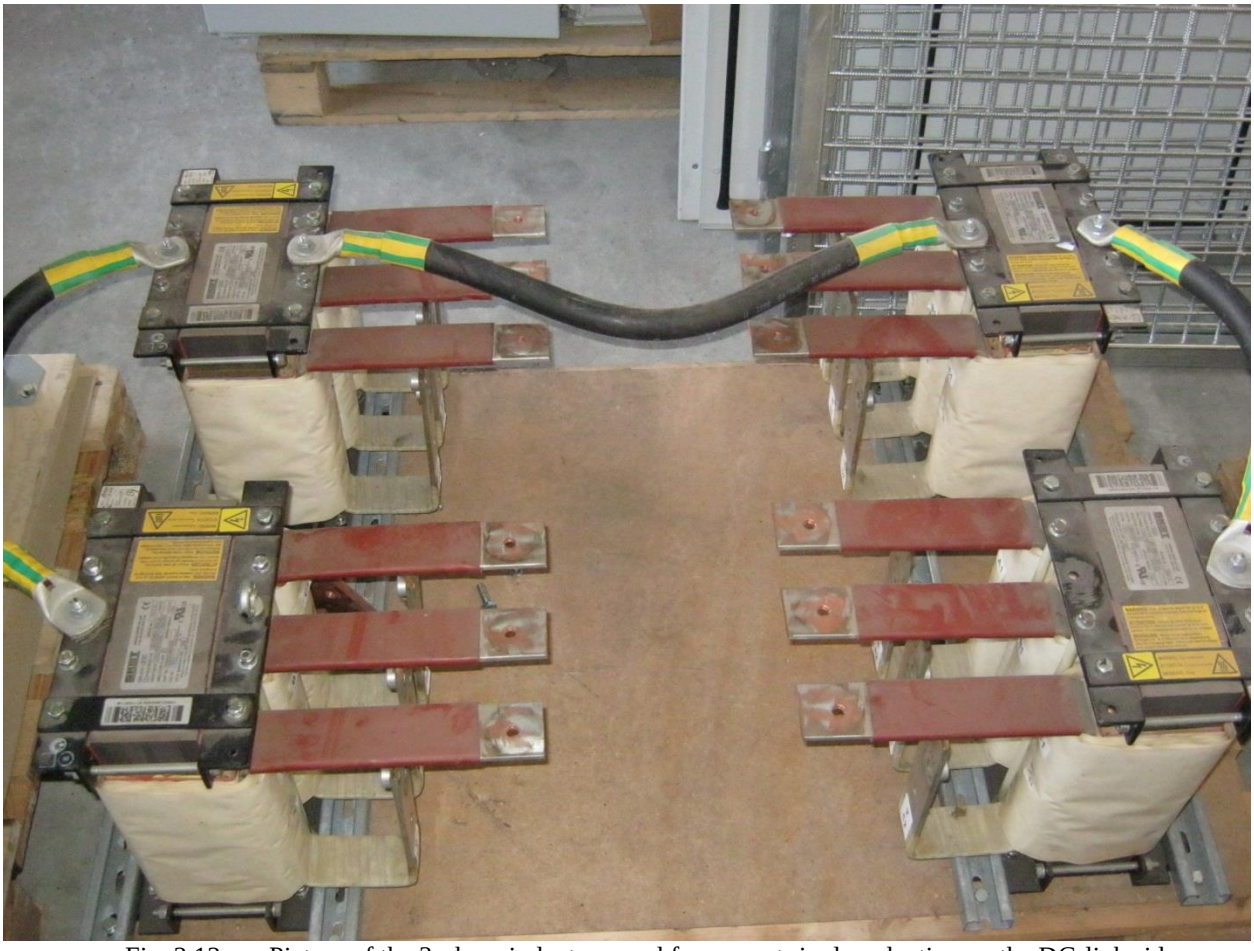

Fig. 2.12. Picture of the 3-phase inductors used for current ripple reduction on the DC-link side

The last items are the inductors for current ripple reduction, and they were designed in the simulation at a rated inductance of 10 (μH) so the current ripple to be less than 5% as stated in the demands of the system, and of course 1500 (A) as their rated current. The inductors were

supply from a company, and they are very compact 3-phase inductors with a phase inductance of 10 (µH) and 1000 (A_{RMS}). A picture of these two (2 by 2 in parallel connected in order to reach the 1500 (A_{RMS}) per phase) inductors is presented in Fig. 2.12.

And of course for close loop control the VLT needed a 1500 (A) current sensor as its feedback after the inductor as passing forward on the circuit line. And also another two sensor for monitoring the 3000 (A) testing current that goes through the DUTs. A picture of each one of these current sensors it is presented in Fig. 2.13.

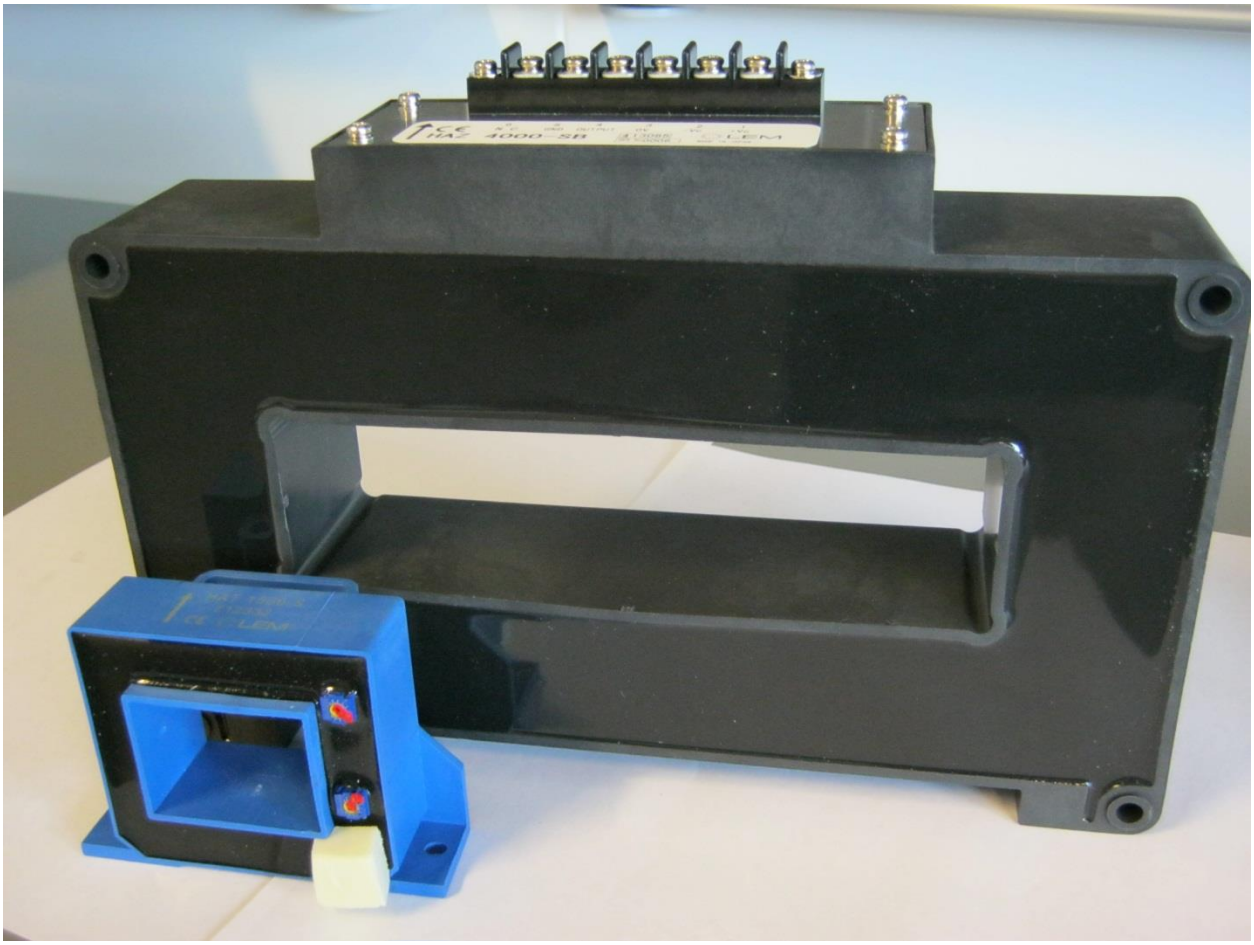

Fig. 2.13. Picture of the 1500 (A) feedback current sensor (blue) and the 4000 (A) monitoring current sensor (black)

2.2.1.3. Testing Side Description

On the testing side (DC-link side) due to the high stored energy in the inductors a varistor was designed and placed in parallel with the testing IGBTs to protect them against high voltage surges. First it was considered to place in parallel with each the inductors, a RCD (Resistor-Capacitor-Diode) snubber to withstands and dissipate the energy of the inductors in case of a fault or an instantaneous open circuit on the DC-link side. But, this idea was more complicated and using more components, than just placing a varistor on the DC-link side.

Due to this high current of 3000 (A) the simulation presented, at an instantaneously open circuit, a raising voltage of 500 (kV) for a very short period of time (μs) on the DC-link side; what will lead to IGBTs destruction. So, therefore the biggest varistor available at that time on the market was chosen. The ratings of the varistor are presented in table 4.

The working principle or the triggering of energy surges inside a varistor is summarized as a graphic diagrams presented in Fig. 2.14. A picture of the varistor is presented in Fig. 2.15 downwards.

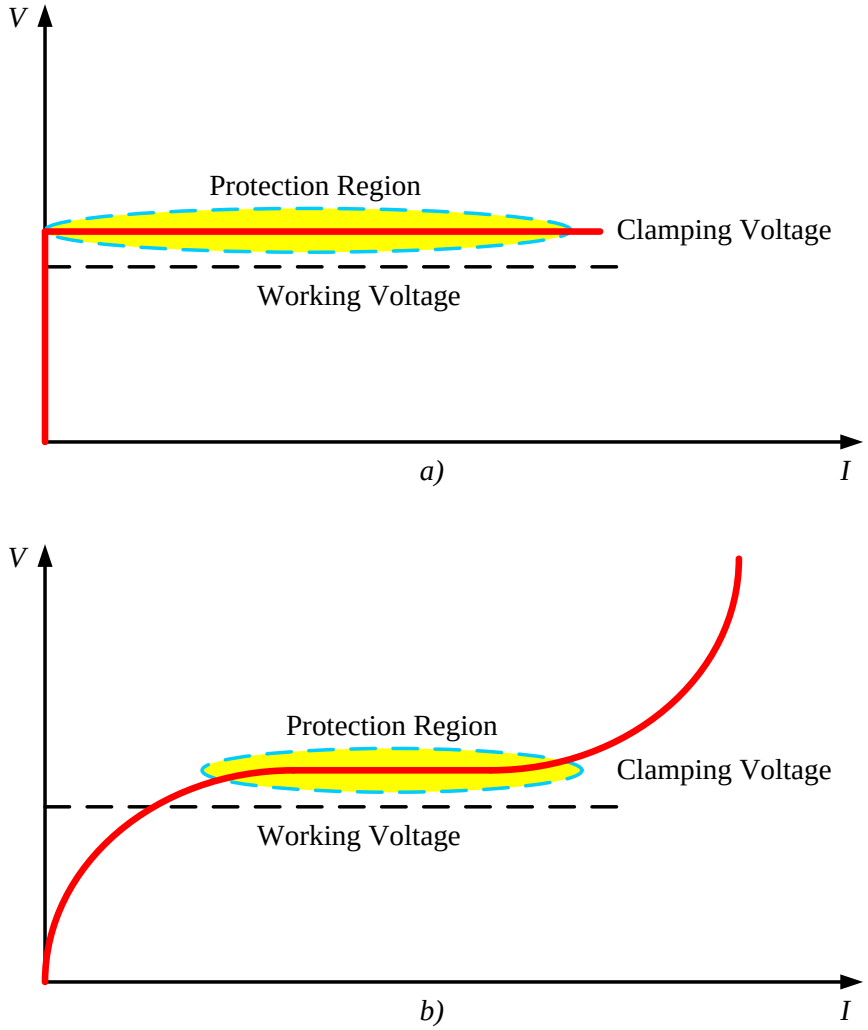

Fig. 2.14. Varistor operation as a) ideal voltage-clamping device and b) Zinc Oxide VDR or Metal Oxide Varistor (MOV) [11]

Table 4. VARISTOR RATED PARAMETERS

Rated parameter	***Value***
Continuous DC voltage	420 (V)
Energy (for 2 ms)	1100 (J)
Clamping voltage	760 (V)
Capacitance (at 1 MHz)	7500 (pF)

Fig. 2.15. Picture of the Varistor used on the DC-link side for surge protection of the IGBTs

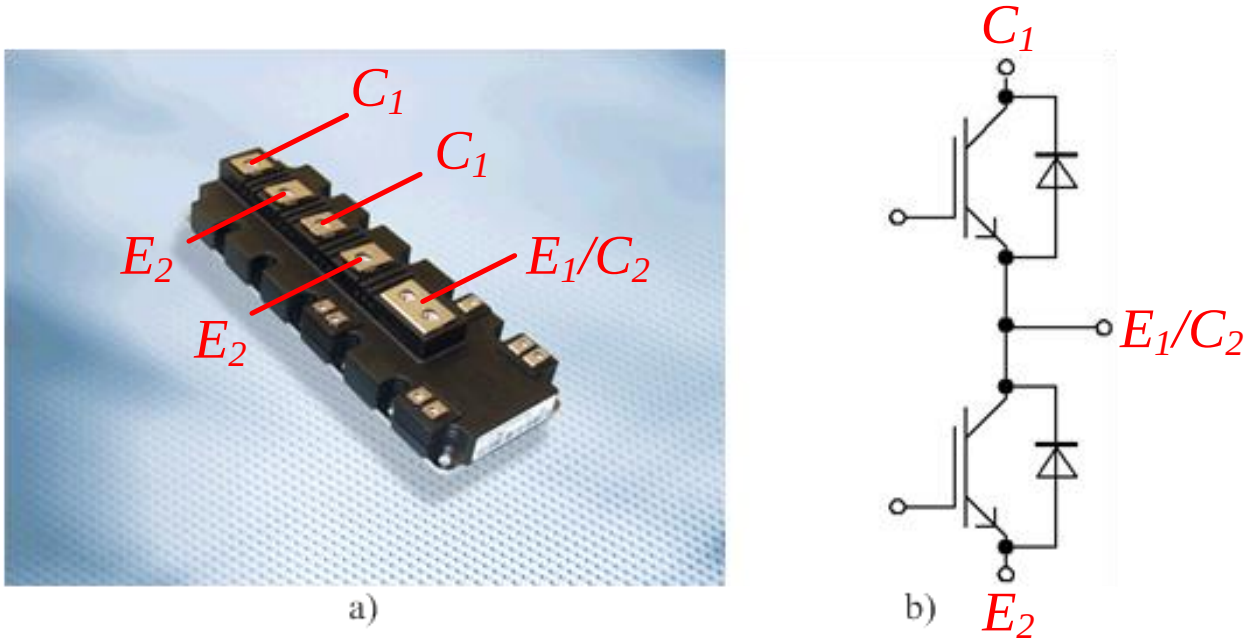

Fig. 2.16. Prime Pack IGBT Power Module a) picture, and b) its connections inside [6]

As stated on the system overview section, the system was designed to be variable in terms of output knowledge, testing parameters and control point of view. Therefore, due to these

statements the system was design to be able to test the Prime Pack P3 IGBT power modules with the rated current of 1000, 1400 or 1700 (A), and also to have some power left for accelerating lifetime testing. These were the main reasons why the system was design to handle a 3000 (A) testing current.

For this project the Danfoss made P3 IGBT power modules with a rated current of 1000 (A) were used. For furthermore details the datasheet of the IGBTs power module made by Infineon is attached in annex 1, being the same as the datasheet for the Danfoss ones. A picture of the testing IGBTs and its inside connection are shown on Fig. 2.16.

2.2.2. Cooling Circuit

The water cooling circuit it contains two different and separated parts, one circuit for control cooling the IGBT power modules and one for the rectifier bridges.

From the rectifier bridge simulated before for the electrical circuit was also simulated the power dissipation of each diode in order to design the cooling system for them. The power dissipation for one diode it is presented in Fig. 2.17 downwards.

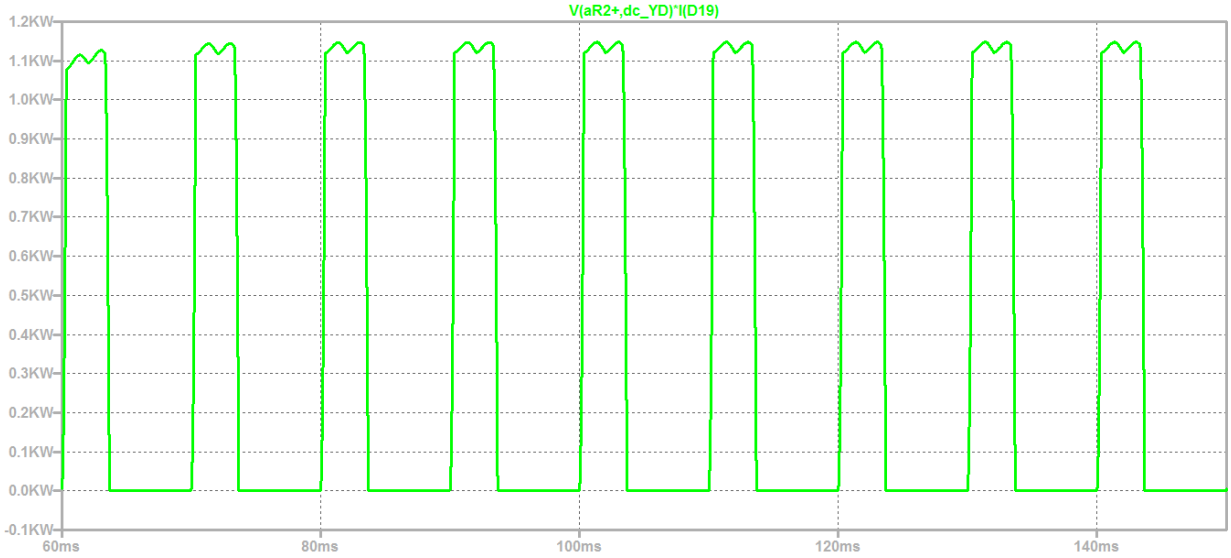

Fig. 2.17. Power dissipation (kW) of one diode from one of the rectifier bridges

From the simulation an average of 376 (W) of dissipating power in one diode of the rectifier bridge was resulting. Therefore the total power dissipation that the cooling circuit has to withstand is 376 (W) times 6 diodes. For this kind of power dissipation, a liquid cooled cold plate for each of the two bridges was chosen for cooling down the diodes. The reason for choosing this kind of cooling plate was the advantage of having the smallest thermal impedance (0.005˚C/W) on the market and useful to our needs. A picture of this liquid cooled cold plate is shown in Fig. 2.18.

Fig. 2.18. Water cooled plate for rectifier bridge cooling

And the second cooling circuit is the one for control cooling the IGBT power module. The shower power was believed to be the most efficient and the best way to cool down these tested IGBTs (DUTs) as explained in the following.

The well-known on the wind industry, the Danfoss patented [12] Shower Power it is clearly the best way to handle the power dissipation generated by the high power converters of each wind turbine, one of them being this project financier, Vestas.

The shower power has a very different way to cool down the surface of the IGBTs. Its name is suggesting that the pumped water it is showered on the surface of the power modules. This shower it is made by many small holes. So, once the cold water hits the surface of the IGBT through one this small hole, and then the heated water immediately gets off the surface through the next small hole, and so forth. A picture of the aluminum plate and the described cooling concept of the shower power are shown in Fig. 2.19.

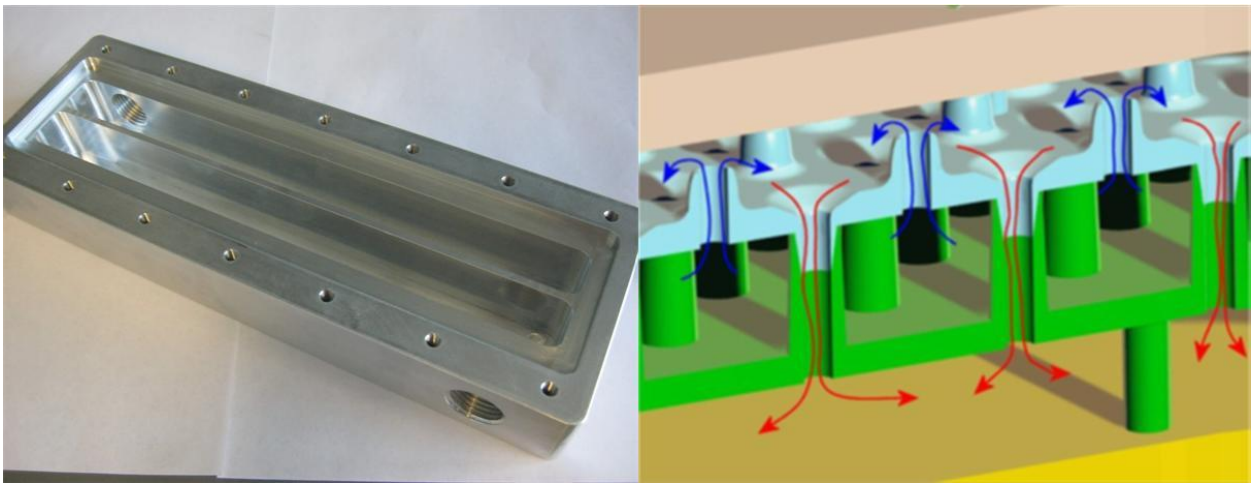

Fig. 2.19. Picture of the aluminum plate on the left and a drawing of the shower power cooling concept patented by Danfoss, on the right [12]

Considering the cooling circuits of both parts of the system, a block diagram of them it is presented in Fig. 2.20. Both systems were designed and analyzed in a more detailed manner by one associate of this project, in terms of pressure drop, pumps, pipes and all the necessary components. For the IGBT power module a 2 (kW) power dissipation was estimated according to some work from other past projects and the designed was made on that description.

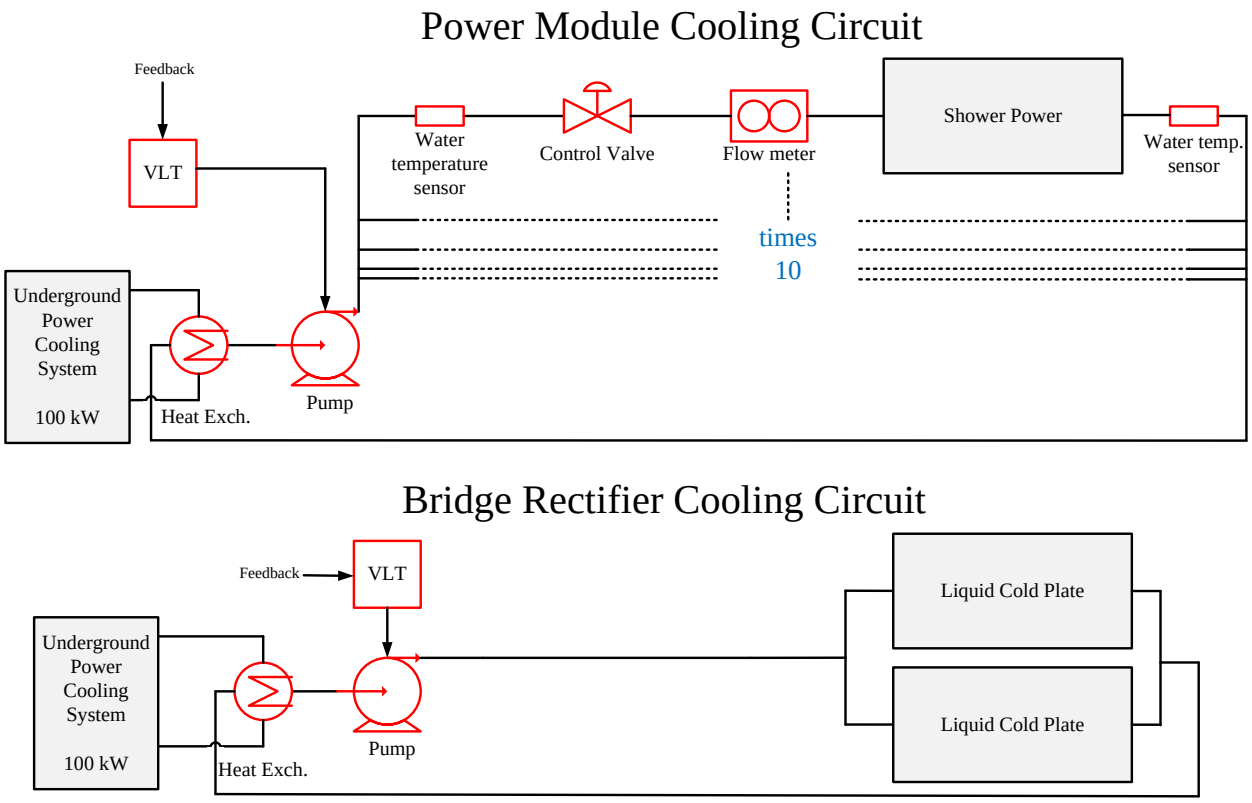

Fig. 2.20. Block diagram of the both separate cooling systems

2.2.3. System Outlook

Most of the components were already presented as pictures in the previous section where the electrical system was designed but the bridge rectifier and the testing IGBTs together with their cooling system needed a chassis where all the components can be easily mounted or replaced when it is needed.

The liquid cooled cold plates on whose surface the diodes are mounted were fixed on a small chassis in order to keep them close to their cooling system and also being moved easily. In Fig. 2.21 the design of this chassis for fitting all of these demands together is presented.

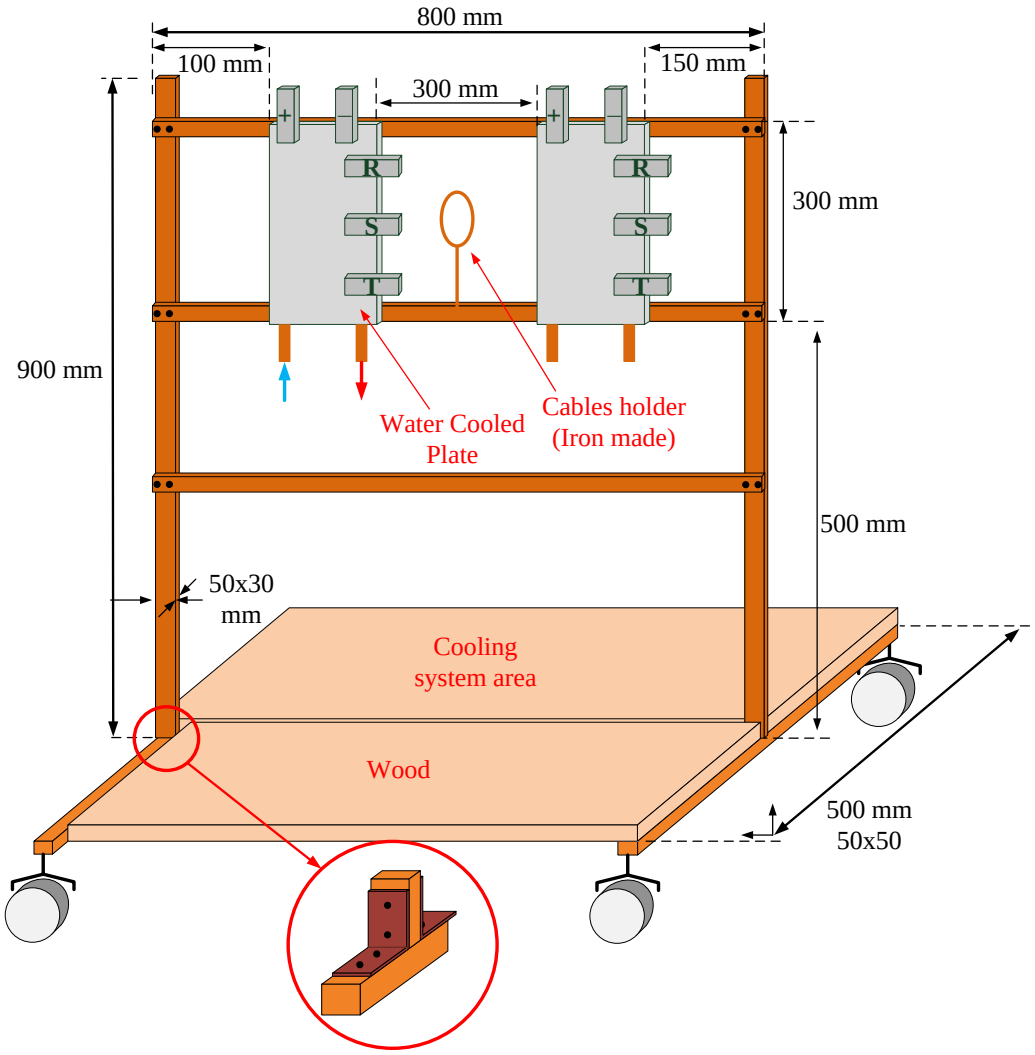

Fig. 2.21. Bridge rectifier chassis for closely fit with its cooling system and easily to move

A picture of the real chassis of the bridge rectifier electrical-cooling system is shown in Fig. 2.22 downwards.

Fig. 2.22. Picture of the bridge rectifier chassis for closely fit with its cooling system and easily to move

And the second and last chassis system was designed for the testing IGBTs power module and having the same abilities like the bridge rectifier chassis discussed earlier in this section. Having ten power modules five by five in series and a very powerful cooling system the chassis for this electrical-cooling system was a lot larger than the one designed for the bridge rectifier.

The designed chassis for the electrical-cooling IGBT system it is presented in Fig. 2.23 in the following and a picture of its real system in Fig. 2.24 In the figure it can be seen that the shower power where the tested IGBTs are going to be mounted, have a diagonal fitting form in order to connect a standard bus-bar between each IGBT power module and also leave some space for their in and out water pipe connections. A diagram for a more easy understanding of this diagonal fitting and the IGBT electrical and their plumbing connections it is presented in Fig. 2.25.

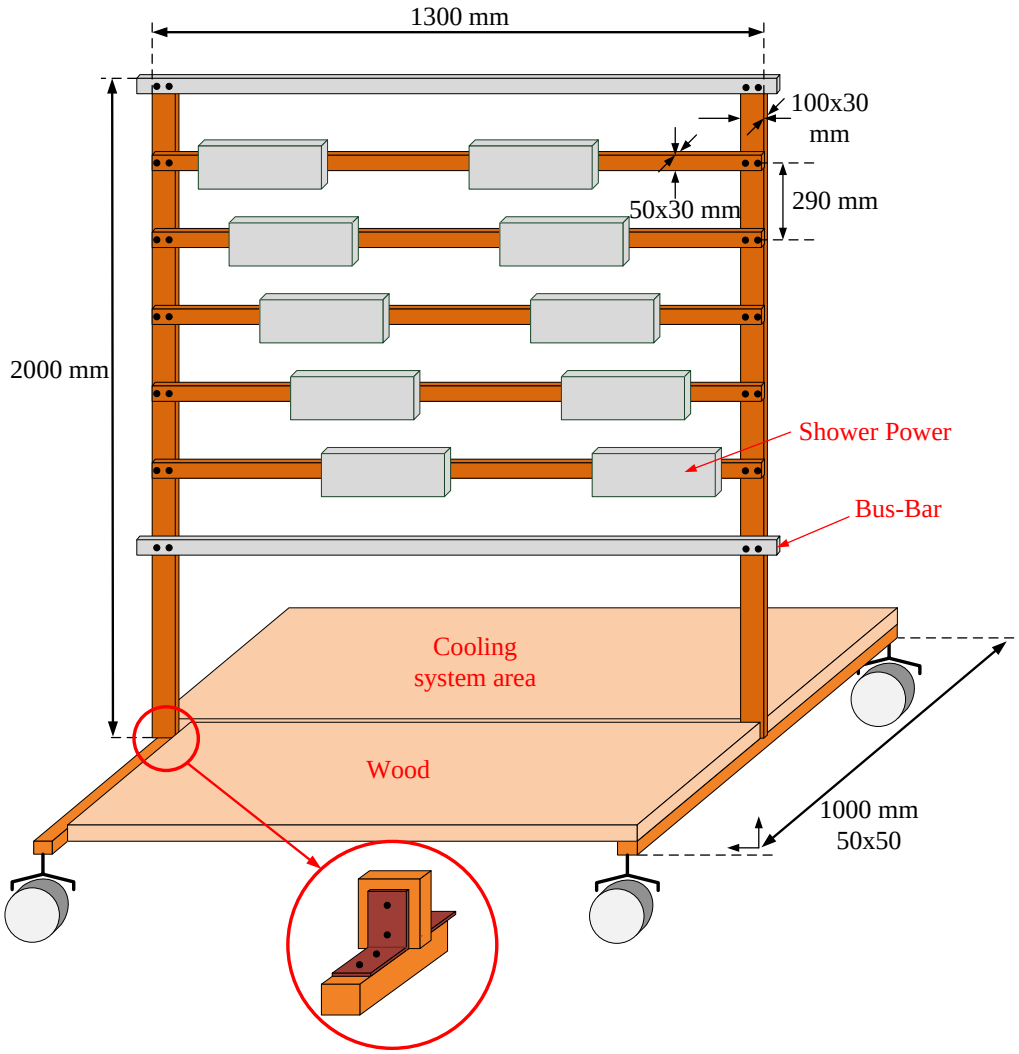

Fig. 2.23. Testing IGBT power module chassis for an easy connection between their electrical and cooling parts

Fig. 2.24. Picture of testing IGBT power module chassis for an easy connection between their electrical and cooling parts

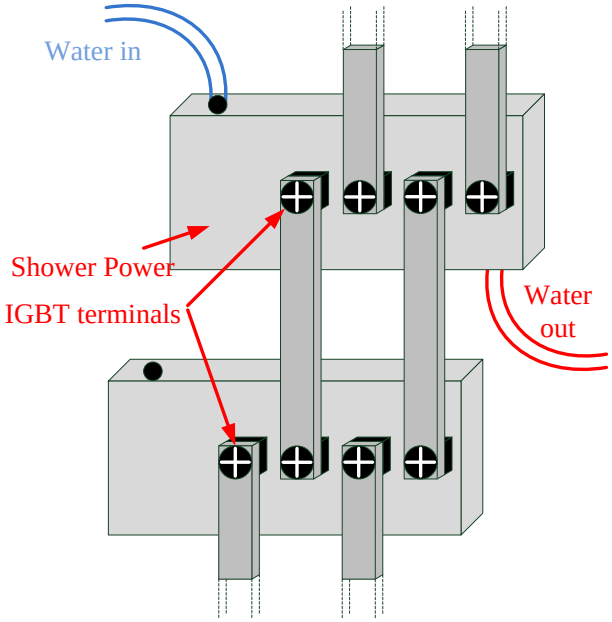

Fig. 2.25. Testing IGBT electrical and cooling systems connections diagram between each other

A picture of this diagonal fitting and the IGBT electrical and their plumbing connections it is presented in Fig. 2.26.

Fig. 2.26. Picture of the IGBT diagonal electrical connections in order to have an easy and variable connection for the cooling items

In summary all the designed components have been order, while others have been custom made or homemade inside the University. The high current cable and bus-bars for electrical connection of the components have been designed and worked out for an easy and variable connection, in order to add the system's more variability in terms of components change space or running capabilities.

After presenting the proposed testing system and analyzing all its components either electrical or cooling item, the report is focused on the next chapter in terms of electrical circuit analysis.

CHAPTER 3 SYSTEM CONTROL AND ANALYSIS

In order to verify and prove that the chosen electrical circuit is the best results generating pattern and the most doable to be implemented in laboratory, this chapter is focused on analyze another three different patterns for the electrical circuit.

3.1. Electrical Circuit Analysis

The system was designed and studied during four different electrical systems. Therefore, all of those four different patterns are discussed in the sections to follow.

These systems are differing from one to another by the removal of one or more components of the electrical circuit. This process concluded the best and available pattern to be built up in the laboratory.

The first system was presented discussed and analyzed on the 2.2.1 section of the previous chapter when the components were designed. The other three patterns analyses are presented further on the following sections.

The second pattern it is using two VLTs for the power supply, one for transformer in order to lower the rated power of the VLT. This pattern it is presented down forwards.

3.1.1. Two VLTs, one for each Transformer

The diagram for this pattern and the simulation doesn't look too much different than the one discussed previously when was used only one VLT. The electrical diagram it is presented in Fig. 3.1.

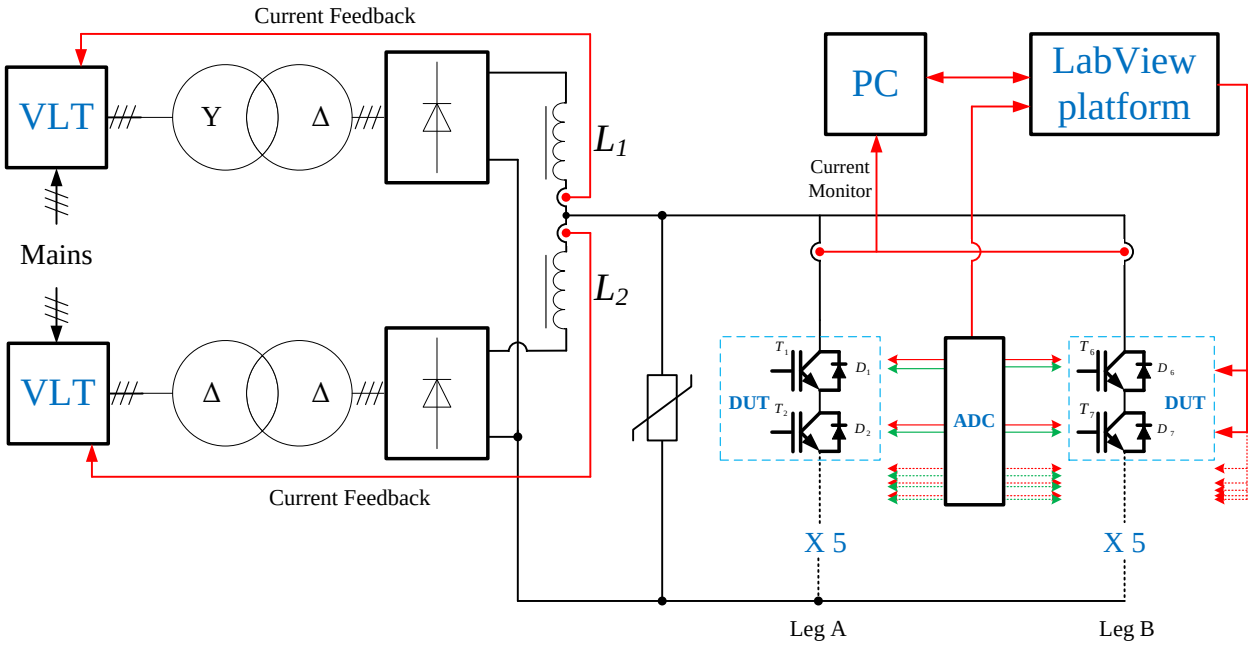

Fig. 3.1. Electrical circuit diagram of the IGBT lifetime (power/thermal cycle) testing system using two VLTs for the power supply source

The working principle of the circuit it is more or less the same as the previously pattern. Two powerful supply sources are connected in parallel in order to rich the demand of 3000 (A) but now the rated power of the VLT it has been lowered. The DUTs are designed 5 by 5 in parallel as was before on the first pattern.

Further on the simulation of this pattern it is presented in order to analyze the differences between the two presented patterns.

3.1.1.1. Simulation

This circuit diagram simulated here it looks the same if the VLTs are synchronized properly when the circuit performers. Therefore, due to this incident the simulation for this pattern it is shown only when the two VLTs are not synchronized whereas a phase shift between one and another's output appears.

Therefore in Fig. 3.2 the current through the inductors and the resulted current through the testing IGBT it is presented.

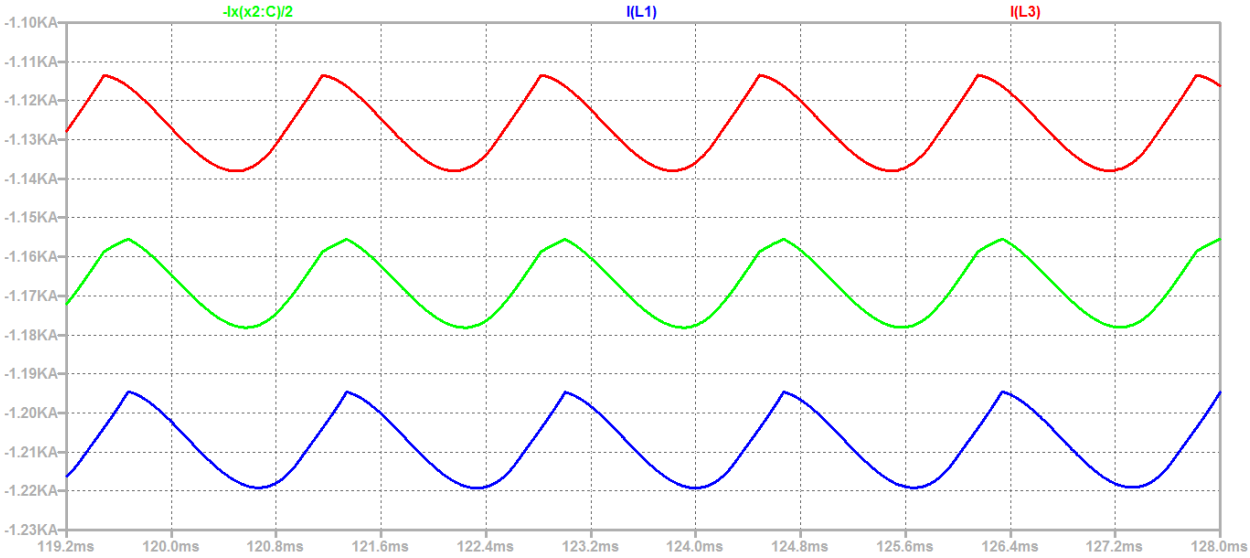

Fig. 3.2. The current ripple through the inductors L1 and L2 (red/top and blue/bottom) and the resulted (green/middle) current after paralleling, divided by 2

On the figure it can be seen that the current through both inductors are more or less in phase, fact that leads to a higher voltage ripple than the one from the previously pattern where the supply voltage of the transformers it is synchronized.

Next, a close look of the voltage drop and current waveforms ripple of the waveforms through the testing IGBT, it is presented on Fig. 3.3.

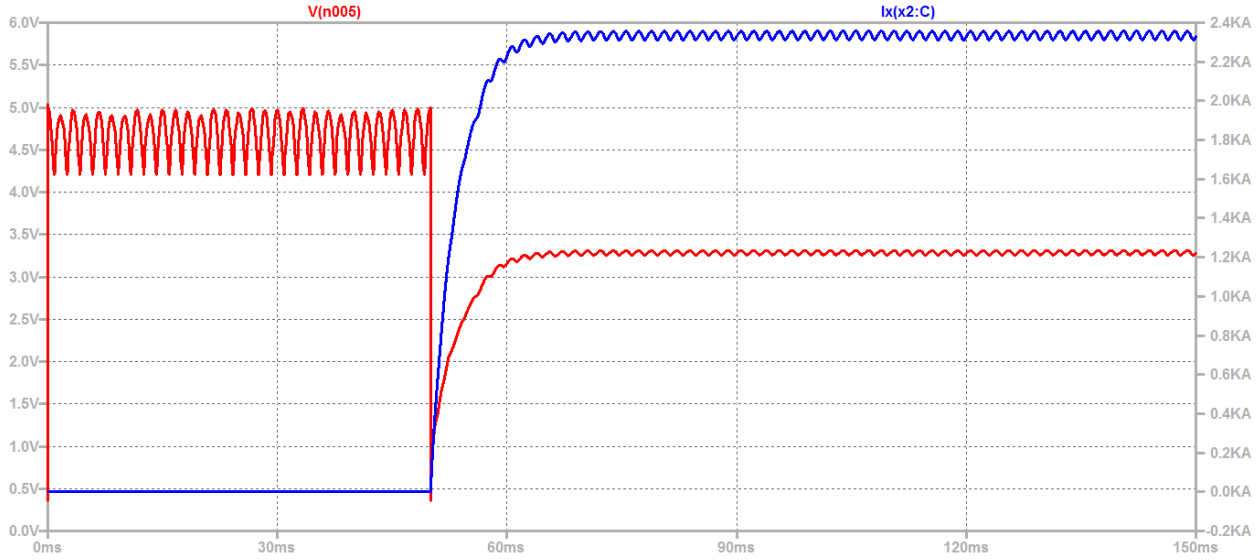

Fig. 3.3. The current on the right scale (blue), and the voltage drop on the left scale (red), through the testing IGBT (DUT) with a turn-on delay of 50 (ms)

In the last figure it is presented the voltage drop and current waveforms ripple through the IGBT in order to show that also this pattern it is within the maximum 5% demand, as it can be seen on Fig. 3.4.

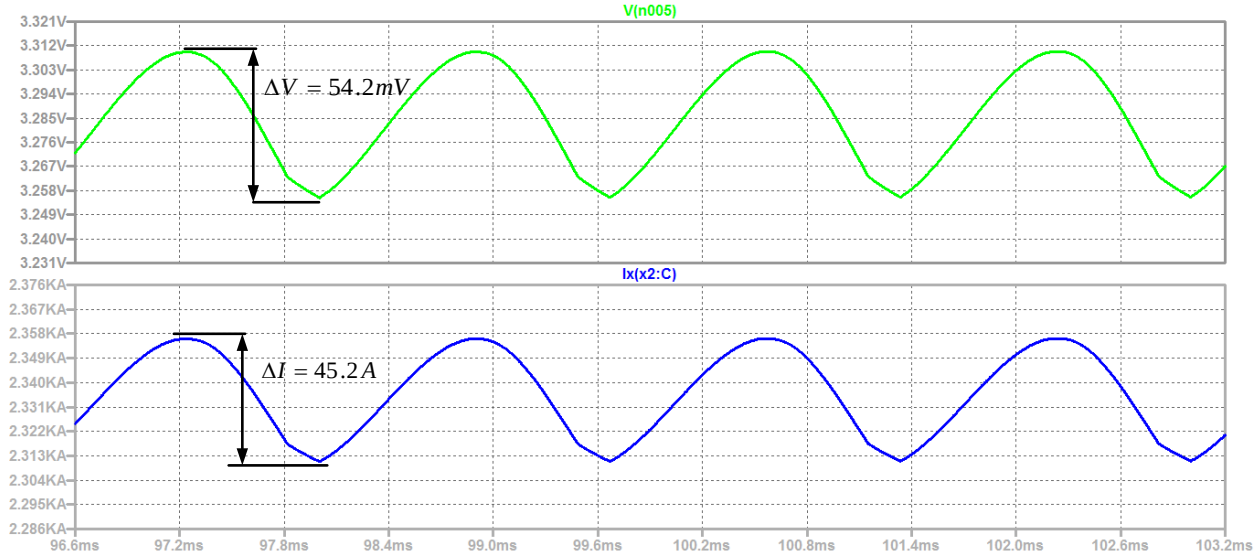

Fig. 3.4. Voltage, on top, and current waveforms ripple on the testing IGBT (DUT)

In the following the voltage drop calculation is analyzed to ensure that the voltage drop has to be smaller or equal to 5%, according the system's demands.

$$\Delta V = \frac{54.2 \cdot 10^{-3}}{3.2} = 0.017 \leq 5\% \qquad (3.1)$$

$$\Delta I = \frac{45.2}{2300} = 0.02 \leq 5\% \tag{3.2}$$

The third pattern to be analyzed it is presented forwards on the following section, and it is basically summed up to use another sets of big switches to turn on and off the current through the testing IGBT power modules.

3.1.2. A set of bigger Switches

The circuit diagram it is presented in Fig. 3.5 downwards and its working principle it is the same considering the power supply side, but on the testing side the current through the DUTs it is switched on and off by another two bigger transistors.

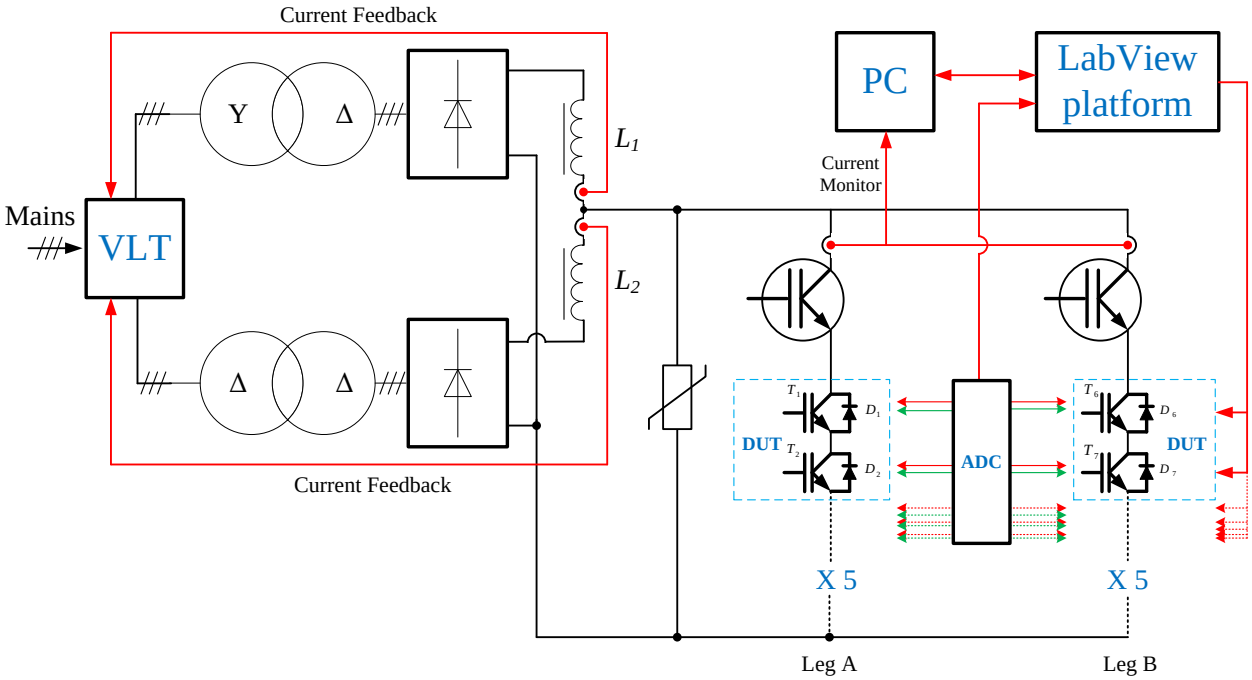

Fig. 3.5. Electrical circuit diagram of the IGBT lifetime (power/thermal cycle) testing system using one VLT for the power supply source and two big switches to turn on/off the testing current

A simulation it is presented in the following to see if there any differences between this and the other two patterns presented previously.

3.1.2.1. Simulation

In order to simulated this new pattern of testing circuit another three IGBTs were implemented into LTSpice along to the circuit proposed as the first pattern. These four IGBTs are all the same, homemade and with the same ratings. Two of these IGBTs were implemented as current switches and the other two were designed to be always turned on IGBTs, as DUTs.

Furthermore the current through the big switches and the voltage drop across them it is presented in Fig. 3.6 downwards, and the LTSpice schematic circuit in annex 3.

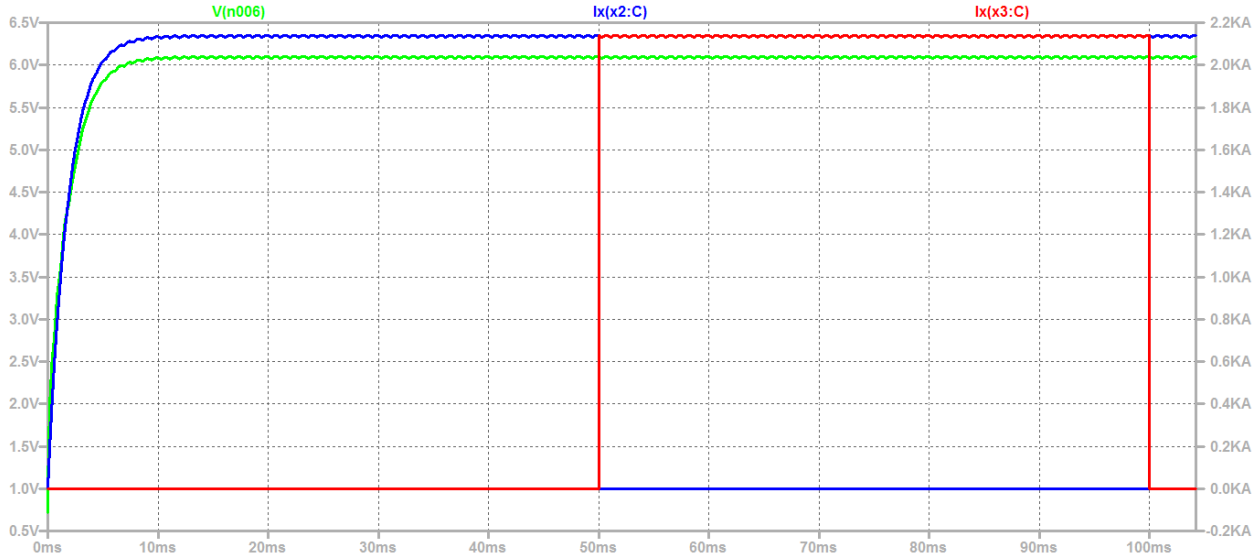

Fig. 3.6. The current on the right scale (red & blue), and the voltage drop on the left scale (green), through the big IGBT switches turned on and off in opposite pattern, for 50 (ms) during a period of 100 (ms)

Considering the current that goes through the testing IGBTs and their voltage and current waveforms ripple, the simulation presents the same results, but with the exception that now the DUTs are tested with a duty cycle of 0.5. In summary this pattern presents the same results like the first presented pattern but this one uses two extra IGBTs for controlling the testing current; option that only adds two more components to the system structure and therefore its nomination to what is the best pattern for implementation, is not so promising.

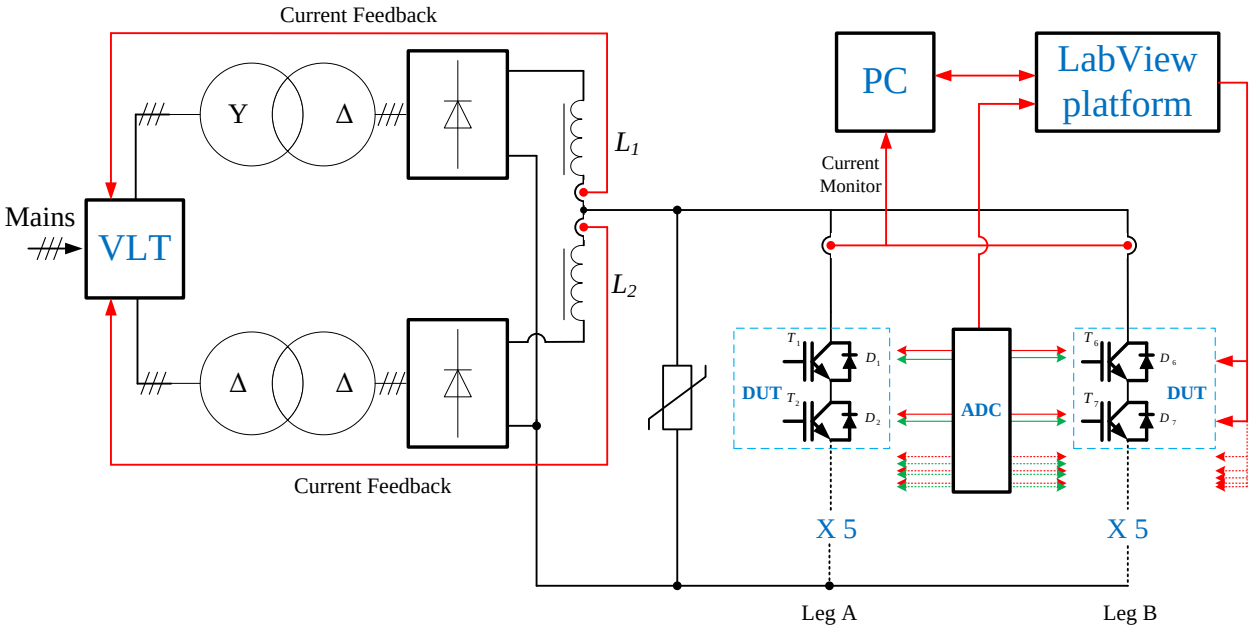

Fig. 3.7. Electrical circuit diagram of the IGBT lifetime (power/thermal cycle) testing system selected for laboratory experiments

The last pattern contents the same circuit on the testing side like the last one just presented, but on the power supply side the circuit it is the same like the second presented pattern, with two VLTs. The simulation and its circuit diagram will present the same results like the previous presented pattern using two VLTs and therefore its results are not shown.

Based on the analysis made on the previous chapter the simplest in size and easiest controlled pattern was chosen; and that is the first presented system with one VLT on the power supply side, and no extra IGBTs for turning on and off the current on the testing side of the system. Furthermore the selected circuit to be implemented and build in the laboratory it is presented once again in Fig. 3.7 downwards.

Alongside with demand of testing the transistors with 30 (s) pulses, another control was implemented to change the gate voltages based on each transistor's voltage drop in order to maintain the same voltage drop across each transistor. But these tasks together with the turn-on signals, tracking the data and the control programing into LabView software were implemented by a PhD student, associate of this project.

CHAPTER 4 EXPERIMENT RESULTS

This chapter was employed to presents and picture all the measurements and tests that have to be done for the designed and developed system.

4.1. Overview

Unfortunately due to some delays of the reliability laboratory construction where this system was set to run, the actual IGBT power modules tests were not able to be done before the submission deadline of this report.

Therefore due to this inconvenience the actual test of the IGBT power modules were not included in this academic report but further planned to be done afterwards and presented on the examination. Furthermore in order to have some electrical data generated by this developed system some measurements were done and presented in the following.

Considering what kind and where some measurements can be withdrawn, the system was also limited due to safety issues or large current power supply. The only option left was to measure only the voltage on the output of the VLT and its line filter, with no current flow.

Further on a picture of the active part of the system that during these measurements it is presented in Fig. 4.1 downwards.

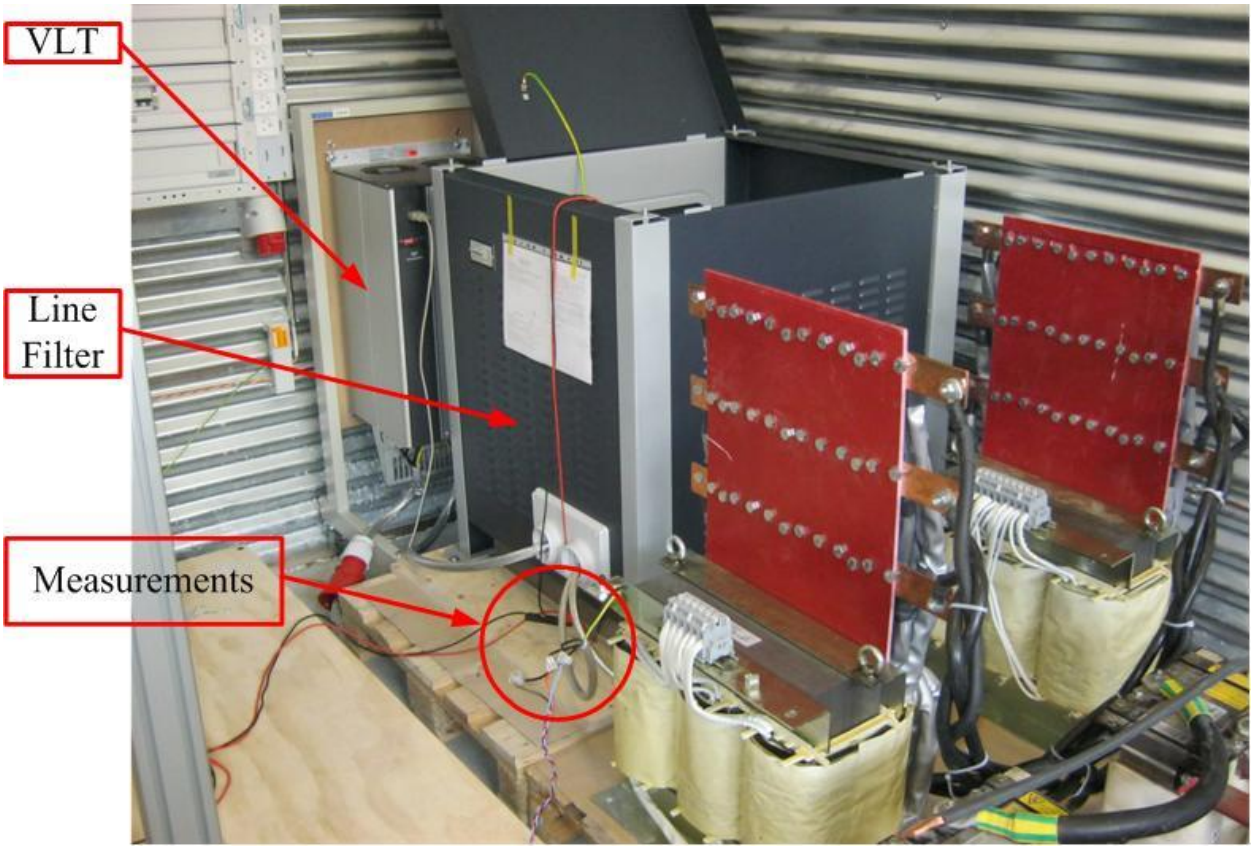

Fig. 4.1. Picture of the active components of the system during the voltage measurements

4.2. Measurements

Measurements were taken starting from the frequency of 10 (Hz) up to 100 (Hz) with a step of 10 (Hz), knowing that the system it is going to run the test with a frequency of 100 (Hz) as mentioned previously in the first chapter where the system's demands are described.

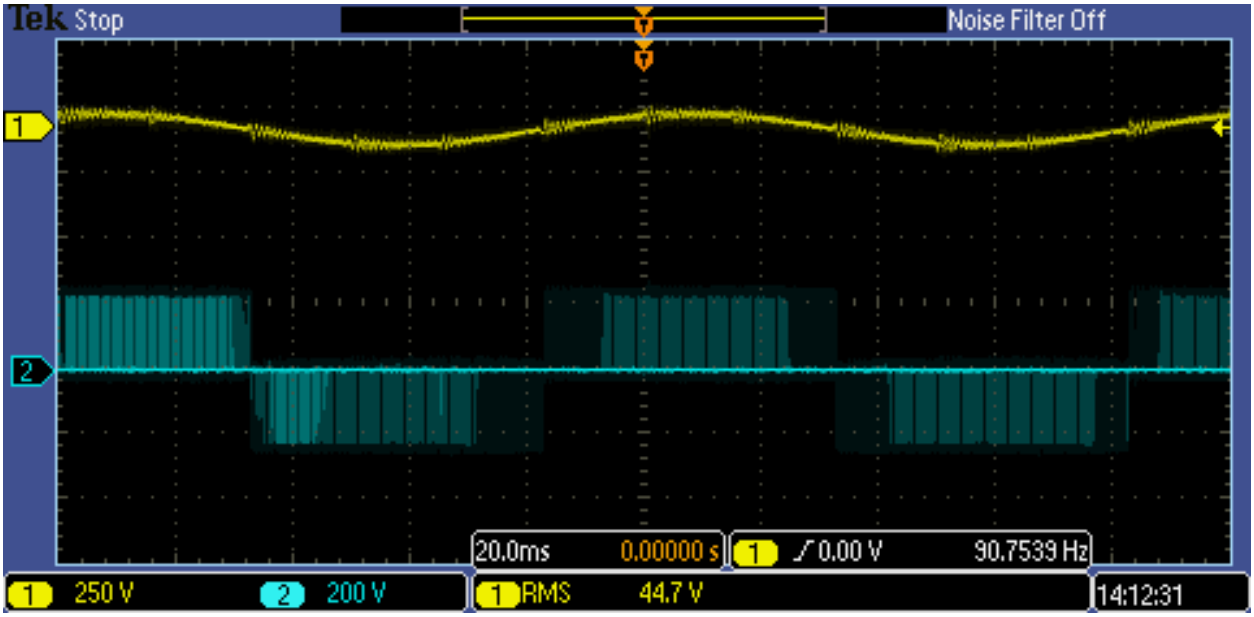

Fig. 4.2. Line voltage measured at the VLT's output (number 2) and the line voltage measured after filtering (number 1) at 10 (Hz)

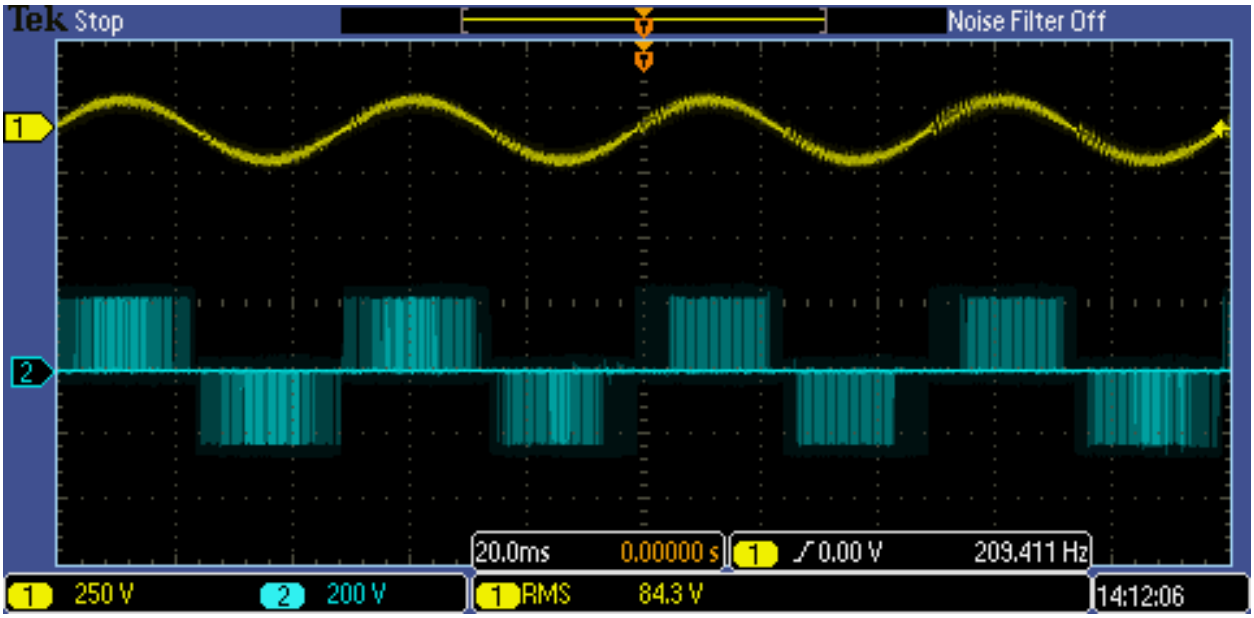

Fig. 4.3. Line voltage measured at the VLT's output (number 2) and the line voltage measured after filtering (number 1) at 20 (Hz)

The chosen switching frequency of the VLT was 3 (kHz) which is actual the minimum switching frequency of the line filter connected on the VLT's output.

In the following the measurements are presented as follows on the next figure starting with the 10 (Hz) measurements as shown in Fig. 4.2.

The 20 (Hz) or second one measured frequency it is presented in Fig. 4.3 and so onwards until the 100 (Hz) frequency.

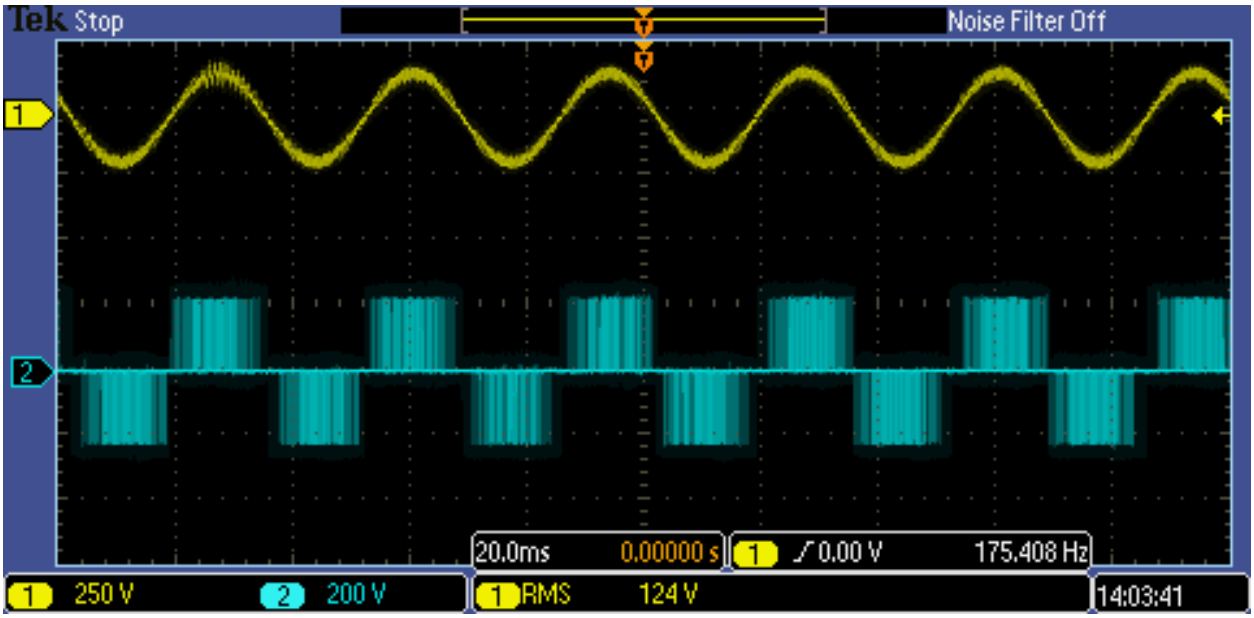

Fig. 4.4. Line voltage measured at the VLT's output (number 2) and the line voltage measured after filtering (number 1) at 30 (Hz)

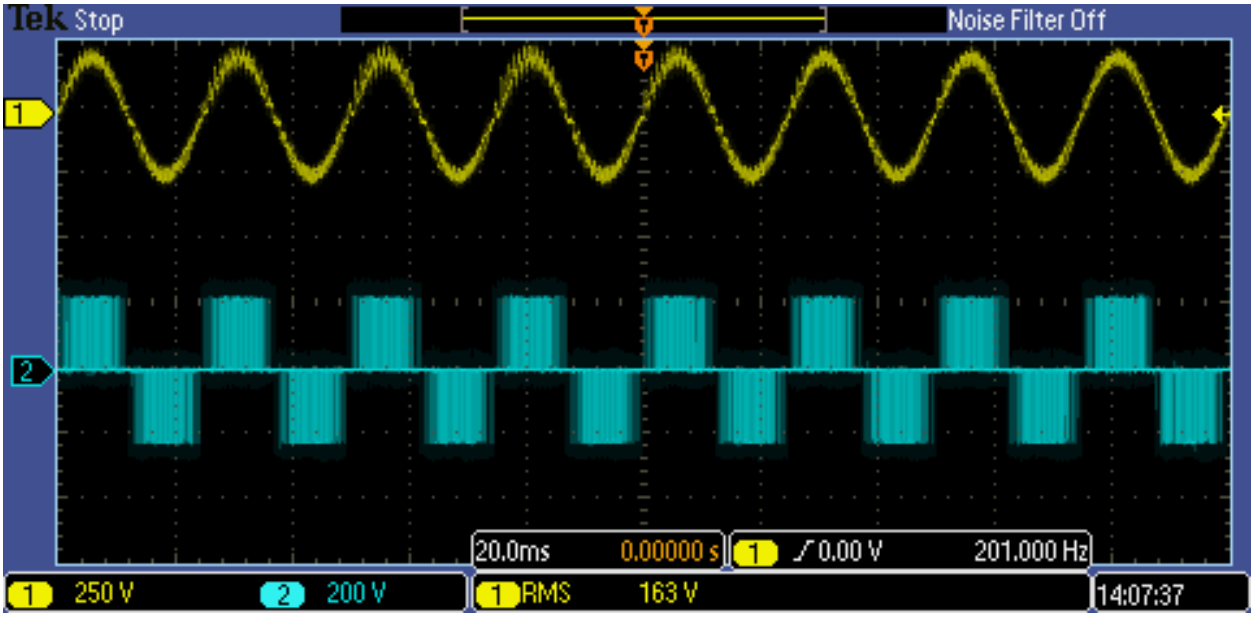

Fig. 4.5. Line voltage measured at the VLT's output (number 2) and the line voltage measured after filtering (number 1) at 40 (Hz)

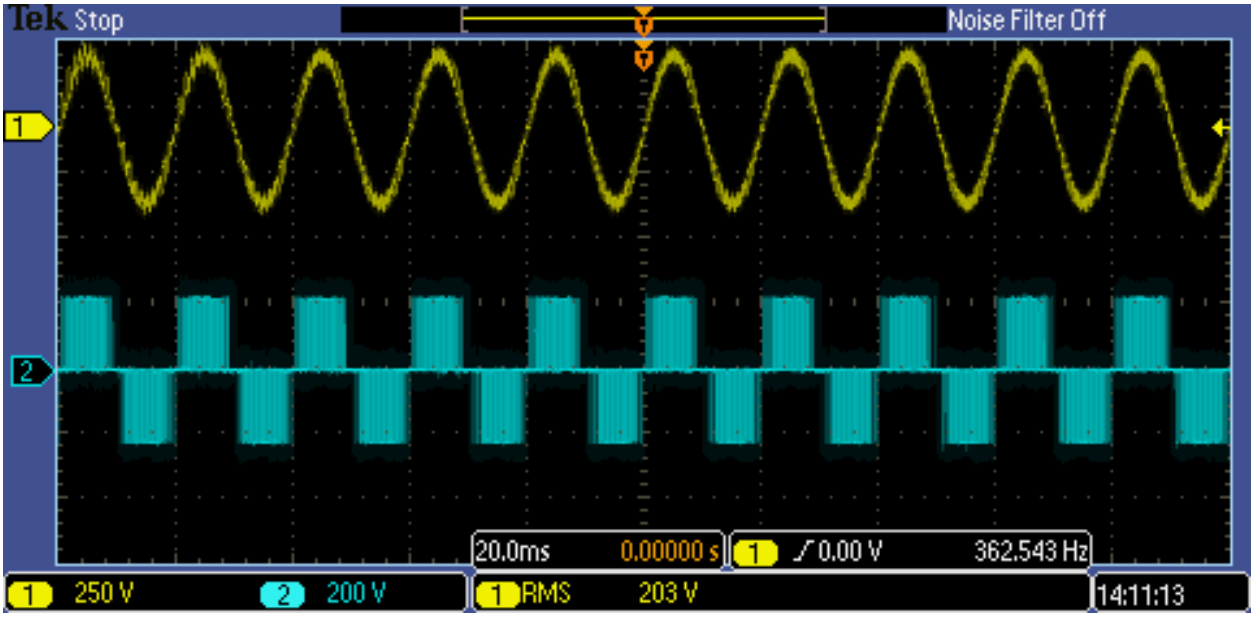

Fig. 4.6. Line voltage measured at the VLT's output (number 2) and the line voltage measured after filtering (number 1) at 50 (Hz)

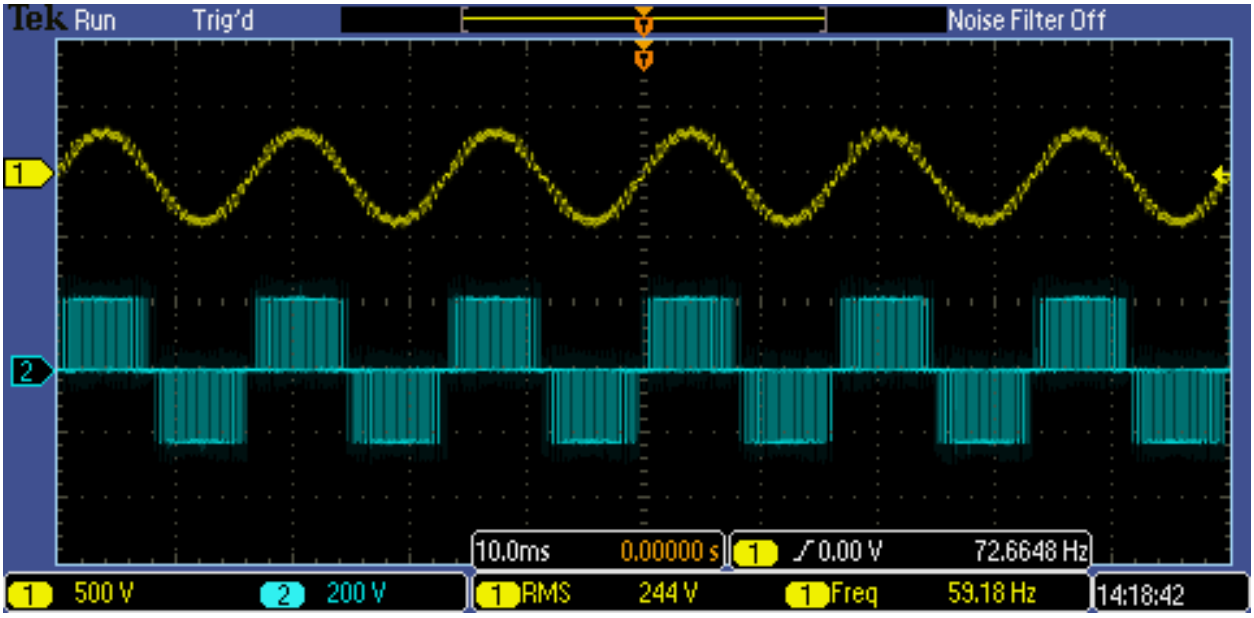

Fig. 4.7. Line voltage measured at the VLT's output (number 2) and the line voltage measured after filtering (number 1) at 60 (Hz)

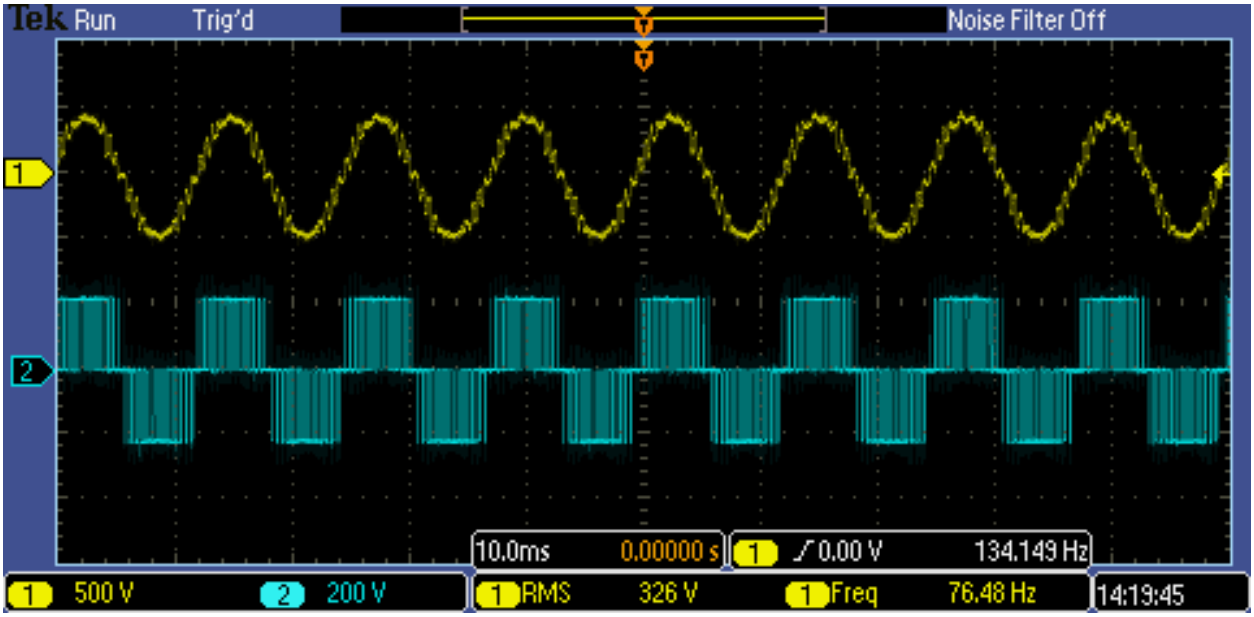

Fig. 4.8. Line voltage measured at the VLT's output (number 2) and the line voltage measured after filtering (number 1) at 70-80 (Hz)

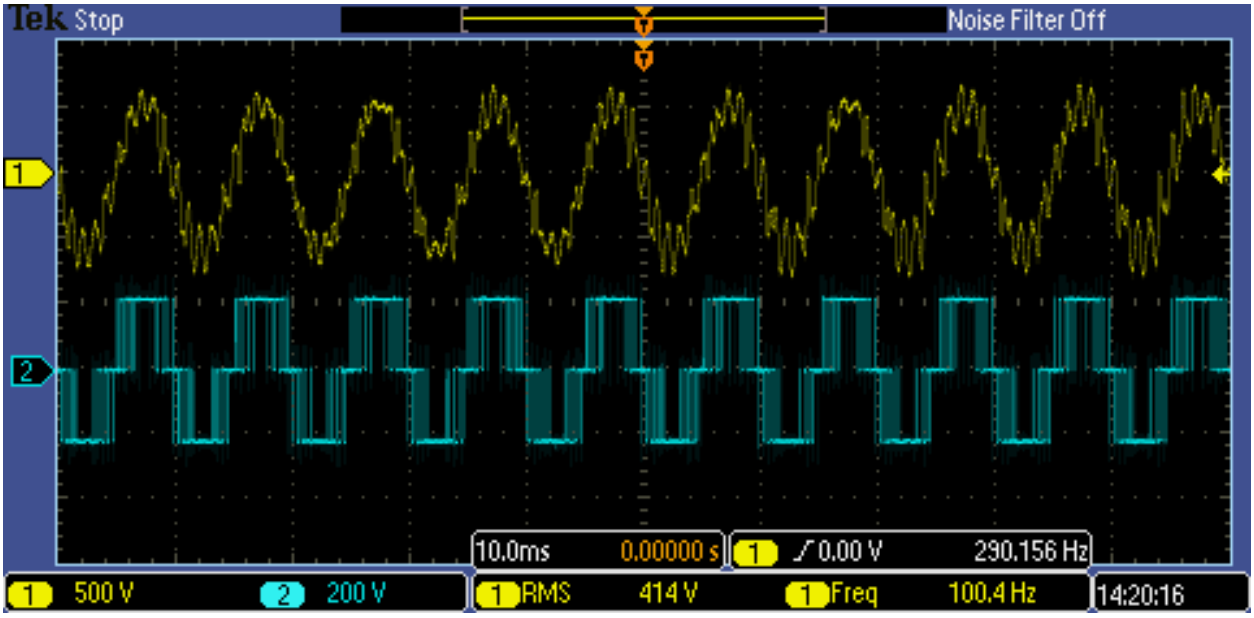

Fig. 4.9. Line voltage measured at the VLT's output (number 2) and the line voltage measured after filtering (number 1) at 100 (Hz)

The measurements of the rest of the components of the system and the actual IGBT power module test are going to be included on the power point presentation due on the examination date.

Based on these measurements in table 5 the whole data was written down in it.

Table 5. MEASUREMENTS DATA

Measurement	*Frequency (Hz)*	*Voltage (RMS)*
1	10	45
2	20	85
3	30	124
4	40	163
5	50	203
6	60	244
7	75	326
8	100	414

CHAPTER 5 CONCLUSIONS AND FURTHER WORKS

5.1. Conclusions

This project is focused on developing a ware out test system for power IGBT module used inside power electronics unit of the nowadays wind turbines.

The proposed electrical test system can be summed up as: two power supply sources were connected in parallel in order to supply a very powerful DC-link at low voltage (around 20 V) and a high testing current (with a range of 1000 up to 3000 Amps). The power supply source it is controlled by a VLT using a current feedback in order to have this wide current testing ability. Also the system is containing a controllable cooling system in order to test the IGBT power module at different ΔTs so the resulted lifetime data through power cycling can draw the expected lifetime starting from the lowest ΔT (around 20 $^{\circ}C$) up until the highest industry demanded ΔT (of around 140 $^{\circ}C$).

The proposed system including the electrical and the cooling system have been designed and simulated where was needed to adjust the rated values of the used items and also the whole hardware part together with building and developing have been implemented and a whole lot of pictures of it were presented in this report.

Unfortunately due to this earlier mentioned laboratory construction and electricity delay, some limitations have edged the experimental tests and only some voltage measurements have been presented in this report.

From these measurements the chosen VLT and the selected line filter it is shown that both items can supply and work, respectively with the rated frequency of the system (of 100 Hz) as intended in the demands section from the first chapter of this report.

The simulation of four different circuit systems gave the knowledge that the transformers paralleling can result in unequal current sharing if they have different impedances.

5.2. Further Works

Further on after submitting the academic report, a whole lot of work it is planned to be done and then again presented during the examination date.

This planned work consists of getting the last components connections and replacements in the laboratory, and then when the electricity and the safety issued are implemented are ready to use; the next tasks of the rest of the system's components are going to be done.

The further work that needs to be done and presented on the examination date it is written done as tasks in the following:

- Available electricity;
- Safety cage issues;
- Control of the VLT and its current feedback;
- Measurements of the rest of the power supply system;
- Building and connecting the cooling components;
- Programing the control for the cooling system (done by an associate);

- Programing the control for the testing IGBT power modules (done by another associate);
- Starting a set of small and low current (500 A) tests;
- Paralleling the diodes bridge; check for equal sharing current;
- Testing the IGBTs with the actual proposed current (2000-3000 A);

The future work that can be done which was not included in this project due to time limitations is to test the IGBT power module under different temperature stresses by changing the ΔT through the controllable cooling system. This kind of work was under limitations in this project knowing that at lower ΔTs the power cycling could last more than a year time.

ANNEX 1 (PRIME PACK IGBT POWER MODULE DATASHEET)

ANNEX 2 (LTSPICE SCHEMATIC SIMULATION)

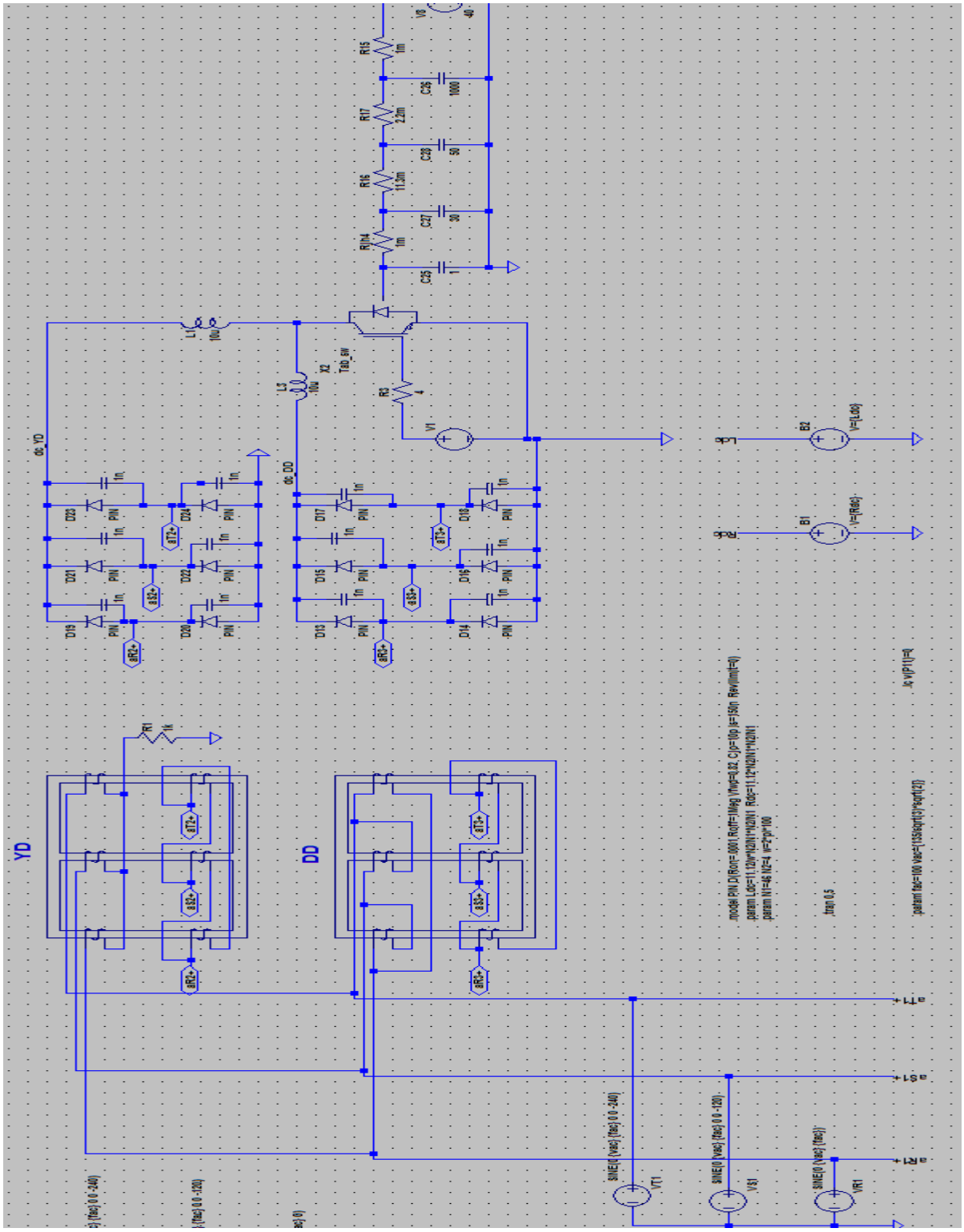

ANNEX 3 (LTSPICE BIG SWITCHES CIRCUIT)

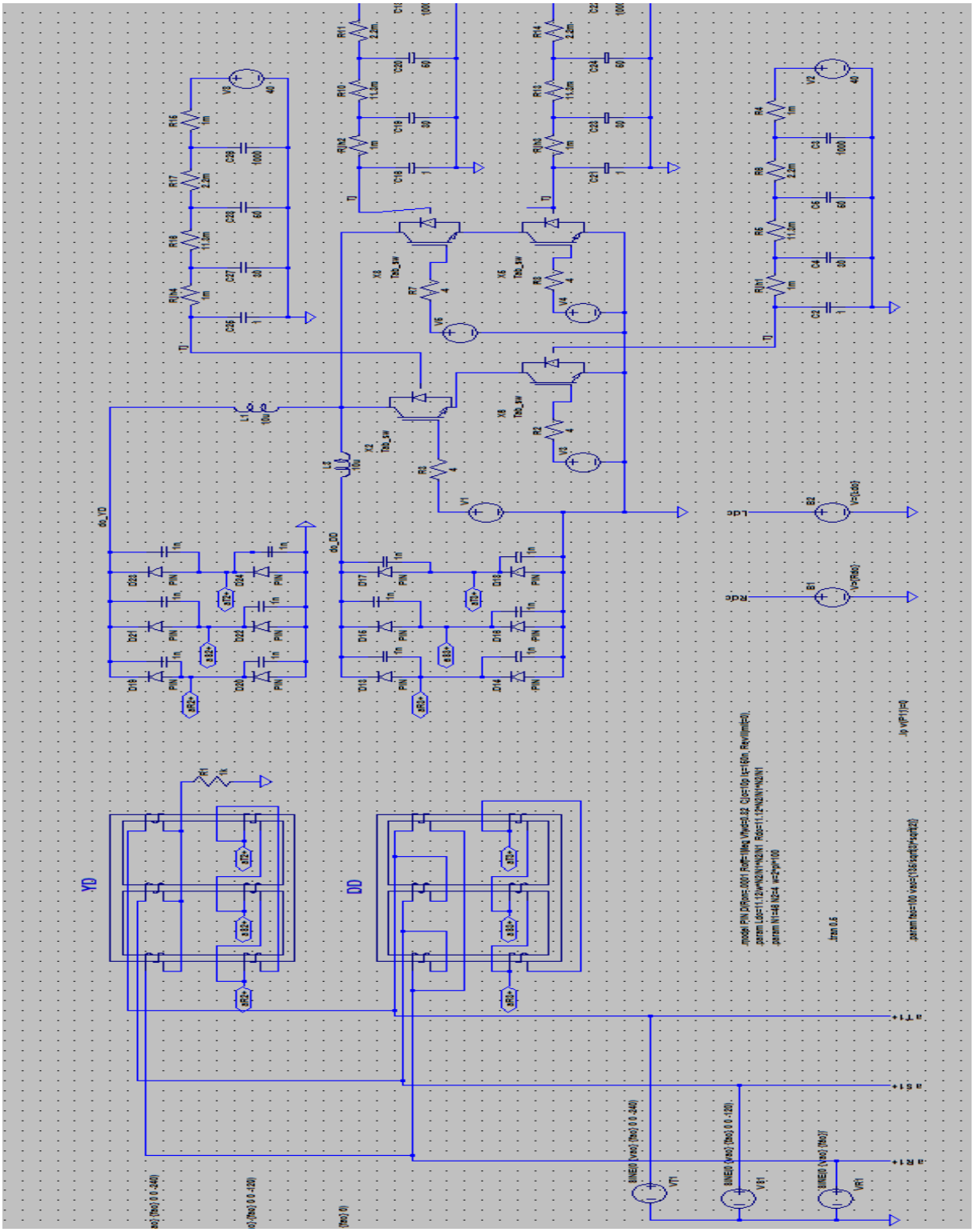

ANNEX 4 (SYMBOLS)

A_{RMS}	Amperes RMS;
C_{th}	Thermal capacitance;
$\cos\varphi$	Power factor;
I_d	DC current;
I_{ll}	Line-to-line primary current of the transformer;
L_s	Leakage inductance of the secondary side;
L_p	Leakage inductance of the primary side;
n_p	Number of the primary side turns;
n_s	Number of the secondary side turns;
P_{max}	Maximum power;
P_{dc}	DC active power;
R_{on}	On resistance of the transistor;
R_{th}	Thermal resistance;
S	Apparent power;
T_a	Ambient temperature;
T_c	Case temperature of the transistor;
T_j	Junction temperature of the transistor;
V_d	DC voltage;
V_{out}	Output voltage;
V_{ll}	Line-to-line primary current of the transformer;
V_{lls}	Line-to-line secondary current of the transformer;
Z_{base}	Primary side impedance of the transformer;
Z_{th}	Thermal impedance;
ΔT	Temperature variation;
ΔV	Voltage waveform ripple;
ΔI	Current waveform ripple;
η	Efficiency;
ω	Radial frequency;

ANNEX 5 (ACRONYMS)

DCB	Direct copper bonded;
DUT	Drive under test;
IGBT	Insulated gate bipolar transistor;
MOSFET	Metal oxide semiconductor field effect transistor;
MOV	Metal oxide varistor;
PC	Computer;
PNPN	Positive-negative-positive-negative junction (transistor);
RCD	Resistor-capacitor-diode (Snubber);
R&D	Research & Develop

REFERENCES

[1] Andris Piebalgs, "Positive developments in wind sector", Opening speech at the EWEC, Brussels, 31 March 2008;

[2] European Commission, "Market Observatory for Energy–Key Figures", June 2011, Source: Eurostat, May 2011, European Union Report;

[3] B. Hendricks, D. Bacon, "2009 Wind Turbine Reliability Workshop", Albuquerque, NM, 18 June 2009;

[4] N. Mohan, T.M. Undeland, W.P. Robbins, "Power electronics, Converters, Applications and Design" Book, second edition, John Willy & Sons Inc., 1995;

[5] Mitsubishi Electric, "Power Module Reliability", www.mitsubishielectric.com;

[6] Infineon, "Technical Information/Datasheet for FF1000R17IE4", 15 March 2012;

[7] Fuji Electric Co., "Chapter 11–Reliability of Power Module", May 2011, web reference;

[8] ON Semiconductor, "Reliability and Quality for IGBTs", November 2011, web reference;

[9] D. Chamund, D. Newcombe, "IGBT Module Reliability", Dynex–Application Note, October 2010;

[10] Visay High Power Products, Schottky Rectifier 400 A, datasheet, 29 April 2008;

[11] B. van Beneden,"Varistor: Ideal Solution to Surge Protection", Power Electronics Technology, Vishay BCcomponents, Malvern Pennsylvania, May 2003, pp 26-30, web reference;

[12] Danfoss Silicon Power website 2013;

Technische Information / technical information

IGBT-Module
IGBT-modules

FF1000R17IE4

PrimePACK™3 Modul und NTC
PrimePACK™3 module and NTC

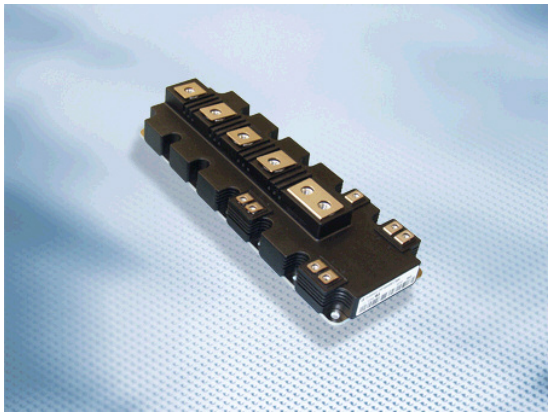

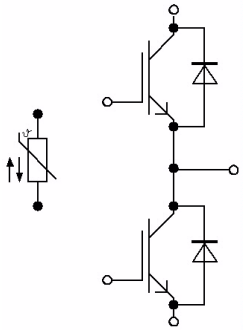

V_{CES} = 1700V
$I_{C\ nom}$ = 1000A / I_{CRM} = 2000A

Typische Anwendungen

- 3-Level-Applikationen
- Hilfsumrichter
- Hochleistungsumrichter
- Motorantriebe
- Windgeneratoren

Typical Applications

- 3-Level-Applications
- Auxiliary Inverters
- High Power Converters
- Motor Drives
- Wind Turbines

Elektrische Eigenschaften

- Erweiterte Sperrschichttemperatur $T_{vj\ op}$
- Große DC-Festigkeit
- Hohe Stromdichte
- Niedrige Schaltverluste
- $T_{vj\ op}$ = 150°C
- niedriges V_{CEsat}

Electrical Features

- Extended Operation Temperature $T_{vj\ op}$
- High DC Stability
- High Current Density
- Low Switching Losses
- $T_{vj\ op}$ = 150°C
- Low V_{CEsat}

Mechanische Eigenschaften

- Gehäuse mit CTI > 400
- Große Luft- und Kriechstrecken
- Hohe Last- und thermische Wechselfestigkeit
- Hohe Leistungsdichte
- Kupferbodenplatte
- Standardgehäuse

Mechanical Features

- Package with CTI > 400
- High Creepage and Clearance Distances
- High Power and Thermal Cycling Capability
- High Power Density
- Copper Base Plate
- Standard Housing

Module Label Code

Barcode Code 128

Sample
00000123456000000000000

DMX - Code

Content of the Code	Digit
Module Serial Number	1 - 5
Module Material Number	6 - 11
Production Order Number	12 - 19
Datecode (Production Year)	20 - 21
Datecode (Production Week)	22 - 23

prepared by: RH	date of publication: 2009-08-28	material no: 32903
approved by: MS	revision: 3.1	

IGBT-Wechselrichter / IGBT-inverter

Höchstzulässige Werte / maximum rated values

Kollektor-Emitter-Sperrspannung collector-emitter voltage	T_{vj} = 25°C	V_{CES}	1700	V
Kollektor-Dauergleichstrom DC-collector current	T_C = 100°C, T_{vj} = 175°C T_C = 25°C, T_{vj} = 175°C	$I_{C\ nom}$ I_C	1000 1390	A A
Periodischer Kollektor Spitzenstrom repetitive peak collector current	t_P = 1 ms	I_{CRM}	2000	A
Gesamt-Verlustleistung total power dissipation	T_C = 25°C, T_{vj} = 175°C	P_{tot}	6,25	kW
Gate-Emitter-Spitzenspannung gate-emitter peak voltage		V_{GES}	+/-20	V

Charakteristische Werte / characteristic values

			min.	typ.	max.	
Kollektor-Emitter Sättigungsspannung collector-emitter saturation voltage	I_C = 1000 A, V_{GE} = 15 V I_C = 1000 A, V_{GE} = 15 V I_C = 1000 A, V_{GE} = 15 V	T_{vj} = 25°C T_{vj} = 125°C T_{vj} = 150°C	$V_{CE\ sat}$	2,00 2,35 2,45	2,45 2,80	V V V
Gate-Schwellenspannung gate threshold voltage	I_C = 36,0 mA, V_{CE} = V_{GE}, T_{vj} = 25°C		V_{GEth}	5,2	5,8	6,4	V
Gateladung gate charge	V_{GE} = -15 V ... +15 V		Q_G		10,0		µC
Interner Gatewiderstand internal gate resistor	T_{vj} = 25°C		R_{Gint}		1,5		Ω
Eingangskapazität input capacitance	f = 1 MHz, T_{vj} = 25°C, V_{CE} = 25 V, V_{GE} = 0 V		C_{ies}		81,0		nF
Rückwirkungskapazität reverse transfer capacitance	f = 1 MHz, T_{vj} = 25°C, V_{CE} = 25 V, V_{GE} = 0 V		C_{res}		2,60		nF
Kollektor-Emitter Reststrom collector-emitter cut-off current	V_{CE} = 1700 V, V_{GE} = 0 V, T_{vj} = 25°C		I_{CES}			5,0	mA
Gate-Emitter Reststrom gate-emitter leakage current	V_{CE} = 0 V, V_{GE} = 20 V, T_{vj} = 25°C		I_{GES}			400	nA
Einschaltverzögerungszeit (ind. Last) turn-on delay time (inductive load)	I_C = 1000 A, V_{CE} = 900 V V_{GE} = ±15 V R_{Gon} = 1,2 Ω	T_{vj} = 25°C T_{vj} = 125°C T_{vj} = 150°C	$t_{d\ on}$		0,55 0,60 0,60		µs µs µs
Anstiegszeit (induktive Last) rise time (inductive load)	I_C = 1000 A, V_{CE} = 900 V V_{GE} = ±15 V R_{Gon} = 1,2 Ω	T_{vj} = 25°C T_{vj} = 125°C T_{vj} = 150°C	t_r		0,10 0,12 0,12		µs µs µs
Abschaltverzögerungszeit (ind. Last) turn-off delay time (inductive load)	I_C = 1000 A, V_{CE} = 900 V V_{GE} = ±15 V R_{Goff} = 1,8 Ω	T_{vj} = 25°C T_{vj} = 125°C T_{vj} = 150°C	$t_{d\ off}$		1,00 1,25 1,30		µs µs µs
Fallzeit (induktive Last) fall time (inductive load)	I_C = 1000 A, V_{CE} = 900 V V_{GE} = ±15 V R_{Goff} = 1,8 Ω	T_{vj} = 25°C T_{vj} = 125°C T_{vj} = 150°C	t_f		0,29 0,50 0,59		µs µs µs
Einschaltverlustenergie pro Puls turn-on energy loss per pulse	I_C = 1000 A, V_{CE} = 900 V, L_S = 30 nH V_{GE} = ±15 V, di/dt = 8000 A/µs (T_{vj}=150°C) R_{Gon} = 1,2 Ω	T_{vj} = 25°C T_{vj} = 125°C T_{vj} = 150°C	E_{on}		265 390 415		mJ mJ mJ
Abschaltverlustenergie pro Puls turn-off energy loss per pulse	I_C = 1000 A, V_{CE} = 900 V, L_S = 30 nH V_{GE} = ±15 V, du/dt = 3000 V/µs (T_{vj}=150°C) R_{Goff} = 1,8 Ω	T_{vj} = 25°C T_{vj} = 125°C T_{vj} = 150°C	E_{off}		200 295 330		mJ mJ mJ
Kurzschlussverhalten SC data	V_{GE} ≤ 15 V, V_{CC} = 1000 V V_{CEmax} = V_{CES} -L_{sCE} ·di/dt	t_P ≤ 10 µs, T_{vj} = 150°C	I_{SC}		4000		A
Innerer Wärmewiderstand thermal resistance, junction to case	pro IGBT / per IGBT		R_{thJC}			24,0	K/kW
Übergangs-Wärmewiderstand thermal resistance, case to heatsink	pro IGBT / per IGBT λ_{Paste} = 1 W/(m·K) / λ_{grease} = 1 W/(m·K)		R_{thCH}		9,00		K/kW

Diode-Wechselrichter / diode-inverter

Höchstzulässige Werte / maximum rated values

Periodische Spitzensperrspannung repetitive peak reverse voltage	T_{vj} = 25°C	V_{RRM}	1700	V
Dauergleichstrom DC forward current		I_F	1000	A
Periodischer Spitzenstrom repetitive peak forward current	t_P = 1 ms	I_{FRM}	2000	A
Grenzlastintegral I²t - value	V_R = 0 V, t_P = 10 ms, T_{vj} = 125°C	I²t	140	kA²s

Charakteristische Werte / characteristic values

			min.	typ.	max.	
Durchlassspannung forward voltage	I_F = 1000 A, V_{GE} = 0 V I_F = 1000 A, V_{GE} = 0 V I_F = 1000 A, V_{GE} = 0 V	T_{vj} = 25°C T_{vj} = 125°C T_{vj} = 150°C	V_F		1,85 1,95 1,95	2,25 2,35	V V V
Rückstromspitze peak reverse recovery current	I_F = 1000 A, - di$_F$/dt = 8000 A/µs (T_{vj}=150°C) V_R = 900 V V_{GE} = -15 V	T_{vj} = 25°C T_{vj} = 125°C T_{vj} = 150°C	I_{RM}		1050 1200 1250		A A A
Sperrverzögerungsladung recovered charge	I_F = 1000 A, - di$_F$/dt = 8000 A/µs (T_{vj}=150°C) V_R = 900 V V_{GE} = -15 V	T_{vj} = 25°C T_{vj} = 125°C T_{vj} = 150°C	Q_r		245 410 480		µC µC µC
Abschaltenergie pro Puls reverse recovery energy	I_F = 1000 A, - di$_F$/dt = 8000 A/µs (T_{vj}=150°C) V_R = 900 V V_{GE} = -15 V	T_{vj} = 25°C T_{vj} = 125°C T_{vj} = 150°C	E_{rec}		115 205 245		mJ mJ mJ
Innerer Wärmewiderstand thermal resistance, junction to case	pro Diode / per diode		R_{thJC}			48,0	K/kW
Übergangs-Wärmewiderstand thermal resistance, case to heatsink	pro Diode / per diode λ_{Paste} = 1 W/(m·K) / λ_{grease} = 1 W/(m·K)		R_{thCH}		18,0		K/kW

NTC-Widerstand / NTC-thermistor

Charakteristische Werte / characteristic values

			min.	typ.	max.	
Nennwiderstand rated resistance	T_C = 25°C	R_{25}		5,00		kΩ
Abweichung von R_{100} deviation of R_{100}	T_C = 100°C, R_{100} = 493 Ω	ΔR/R	-5		5	%
Verlustleistung power dissipation	T_C = 25°C	P_{25}			20,0	mW
B-Wert B-value	$R_2 = R_{25} \exp [B_{25/50}(1/T_2 - 1/(298,15\ K))]$	$B_{25/50}$		3375		K
B-Wert B-value	$R_2 = R_{25} \exp [B_{25/80}(1/T_2 - 1/(298,15\ K))]$	$B_{25/80}$		3411		K
B-Wert B-value	$R_2 = R_{25} \exp [B_{25/100}(1/T_2 - 1/(298,15\ K))]$	$B_{25/100}$		3433		K

Angaben gemäß gültiger Application Note.
Specification according to the valid application note.

Modul / module

Isolations-Prüfspannung insulation test voltage	RMS, f = 50 Hz, t = 1 min.	V_{ISOL}		4,0		kV
Material Modulgrundplatte material of module baseplate				Cu		
Material für innere Isolation material for internal insulation				Al_2O_3		
Kriechstrecke creepage distance	Kontakt - Kühlkörper / terminal to heatsink Kontakt - Kontakt / terminal to terminal			33,0 33,0		mm
Luftstrecke clearance distance	Kontakt - Kühlkörper / terminal to heatsink Kontakt - Kontakt / terminal to terminal			19,0 19,0		mm
Vergleichszahl der Kriechwegbildung comparative tracking index		CTI		> 400		
			min.	typ.	max.	
Übergangs-Wärmewiderstand thermal resistance, case to heatsink	pro Modul / per module λ_{Paste} = 1 W/(m·K) / λ_{grease} = 1 W/(m·K)	R_{thCH}		3,00		K/kW
Modulinduktivität stray inductance module		L_{sCE}		10		nH
Modulleitungswiderstand, Anschlüsse - Chip module lead resistance, terminals - chip	T_C = 25°C, pro Schalter / per switch	$R_{CC'+EE'}$		0,20		mΩ
Höchstzulässige Sperrschichttemperatur maximum junction temperature	Wechselrichter, Brems-Chopper / Inverter, Brake-Chopper	$T_{vj\ max}$			175	°C
Temperatur im Schaltbetrieb temperature under switching conditions	Wechselrichter, Brems-Chopper / Inverter, Brake-Chopper	$T_{vj\ op}$	-40		150	°C
Lagertemperatur storage temperature		T_{stg}	-40		150	°C
Anzugsdrehmoment f. mech. Befestigung mounting torque	Schraube M5 - Montage gem. gültiger Applikation Note screw M5 - mounting according to valid application note	M	3,00	-	6,00	Nm
Anzugsdrehmoment f. elektr. Anschlüsse terminal connection torque	Schraube M4 - Montage gem. gültiger Applikation Note screw M4 - mounting according to valid application note Schraube M8 - Montage gem. gültiger Applikation Note screw M8 - mounting according to valid application note	M	1,8 8,0	- -	2,1 10	Nm Nm
Gewicht weight		G		1200		g

Ausgangskennlinie IGBT-Wechselr. (typisch)
output characteristic IGBT-inverter (typical)
$I_C = f(V_{CE})$
V_{GE} = 15 V

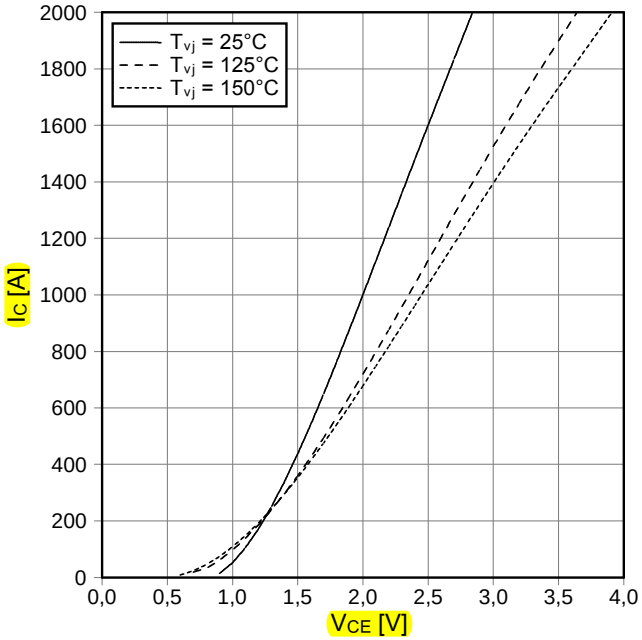

Ausgangskennlinienfeld IGBT-Wechselr. (typisch)
output characteristic IGBT-inverter (typical)
$I_C = f(V_{CE})$
T_{vj} = 150°C

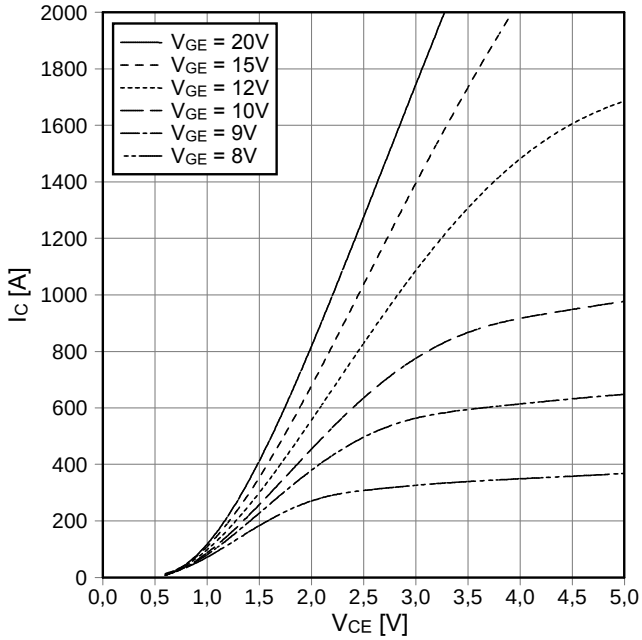

Übertragungscharakteristik IGBT-Wechselr. (typisch)
transfer characteristic IGBT-inverter (typical)
$I_C = f(V_{GE})$
V_{CE} = 20 V

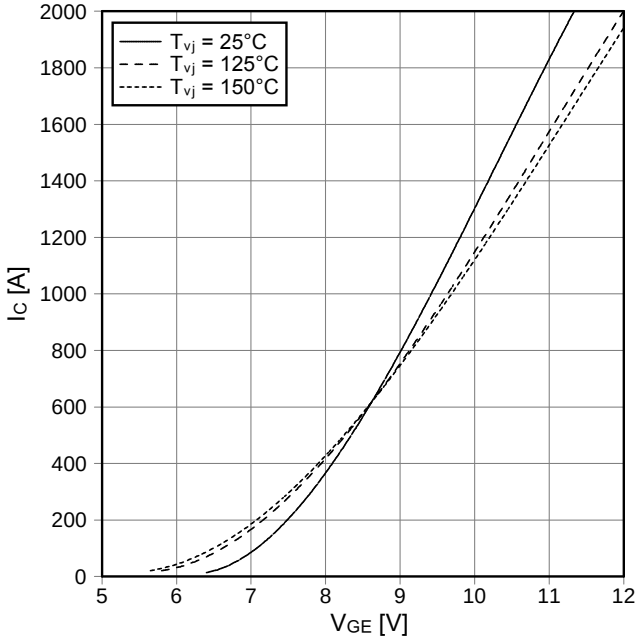

Schaltverluste IGBT-Wechselr. (typisch)
switching losses IGBT-inverter (typical)
$E_{on} = f(I_C)$, $E_{off} = f(I_C)$
V_{GE} = ±15 V, R_{Gon} = 1.2 Ω, R_{Goff} = 1.8 Ω, V_{CE} = 900 V

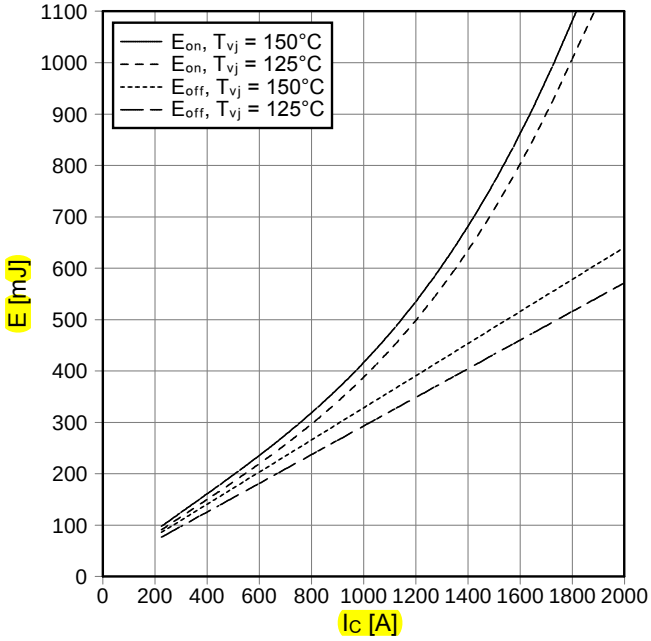

prepared by: RH	date of publication: 2009-08-28
approved by: MS	revision: 3.1

Schaltverluste IGBT-Wechselr. (typisch)
switching losses IGBT-Inverter (typical)
$E_{on} = f(R_G)$, $E_{off} = f(R_G)$
V_{GE} = ±15 V, I_C = 1000 A, V_{CE} = 900 V

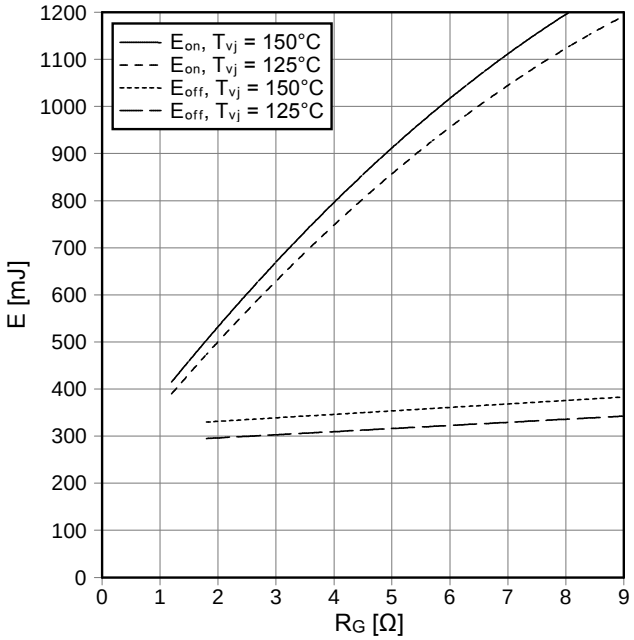

Transienter Wärmewiderstand IGBT-Wechselr.
transient thermal impedance IGBT-inverter
$Z_{thJC} = f(t)$

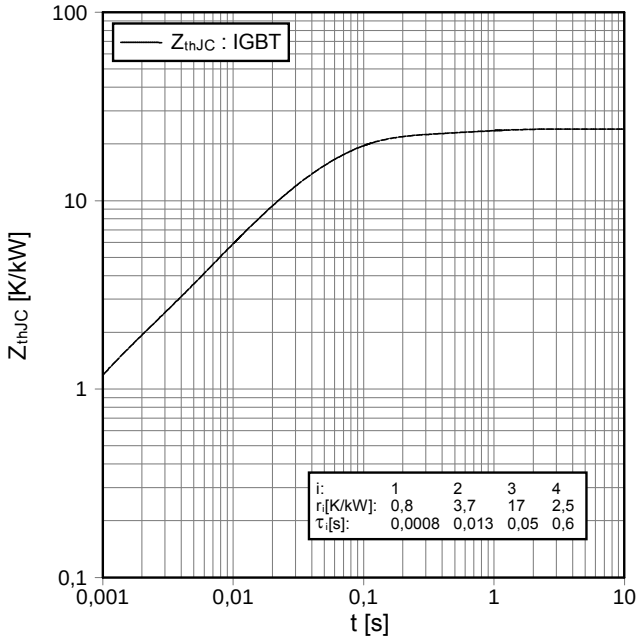

Sicherer Rückwärts-Arbeitsbereich IGBT-Wr. (RBSOA)
reverse bias safe operating area IGBT-inv. (RBSOA)
$I_C = f(V_{CE})$
V_{GE} = ±15 V, R_{Goff} = 1.8 Ω, T_{vj} = 150°C

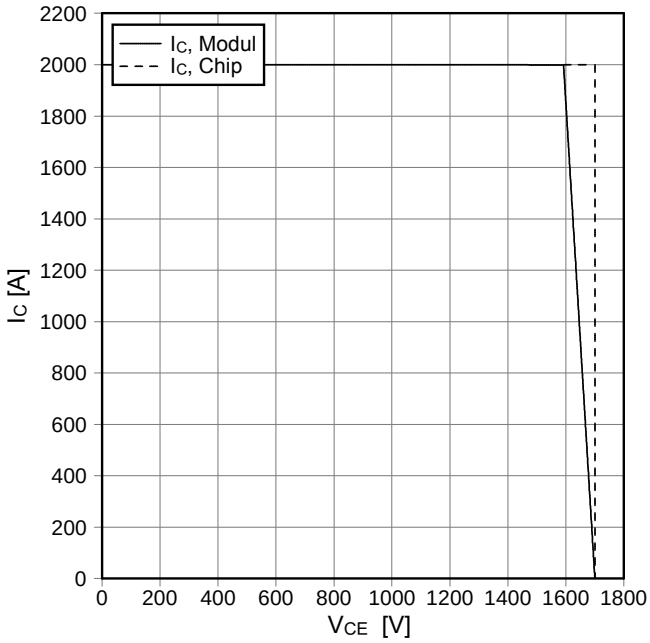

Durchlasskennlinie der Diode-Wechselr. (typisch)
forward characteristic of diode-inverter (typical)
$I_F = f(V_F)$

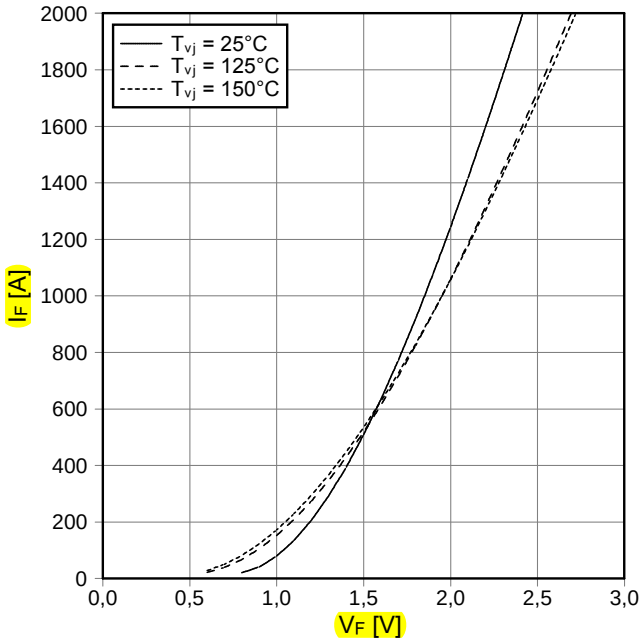

prepared by: RH	date of publication: 2009-08-28
approved by: MS	revision: 3.1

Schaltverluste Diode-Wechselr. (typisch)
switching losses diode-inverter (typical)
$E_{rec} = f(I_F)$
$R_{Gon} = 1.2\ \Omega$, $V_{CE} = 900$ V

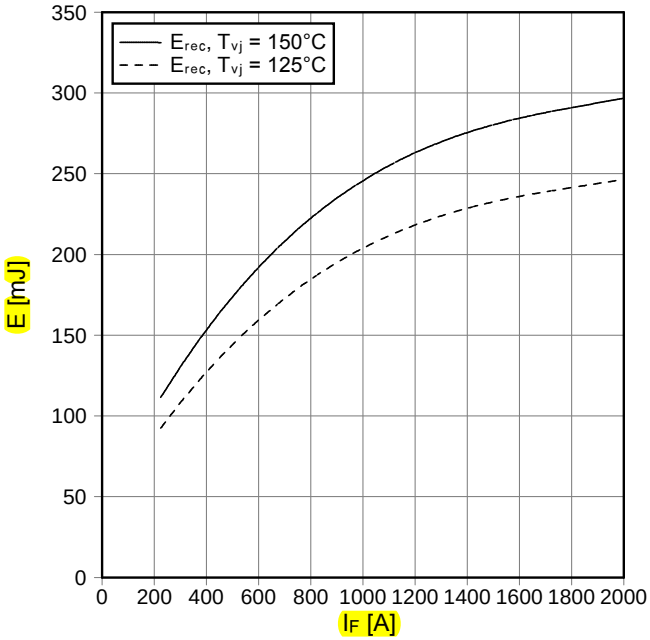

Schaltverluste Diode-Wechselr. (typisch)
switching losses diode-inverter (typical)
$E_{rec} = f(R_G)$
$I_F = 1000$ A, $V_{CE} = 900$ V

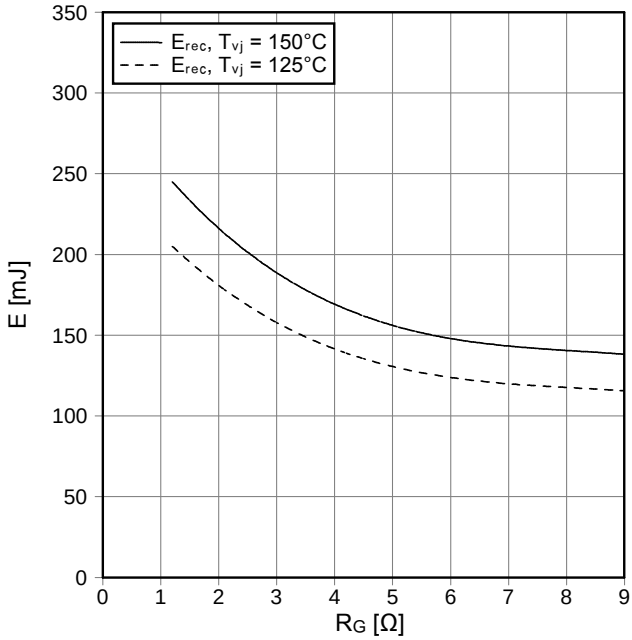

Transienter Wärmewiderstand Diode-Wechselr.
transient thermal impedance diode-inverter
$Z_{thJC} = f(t)$

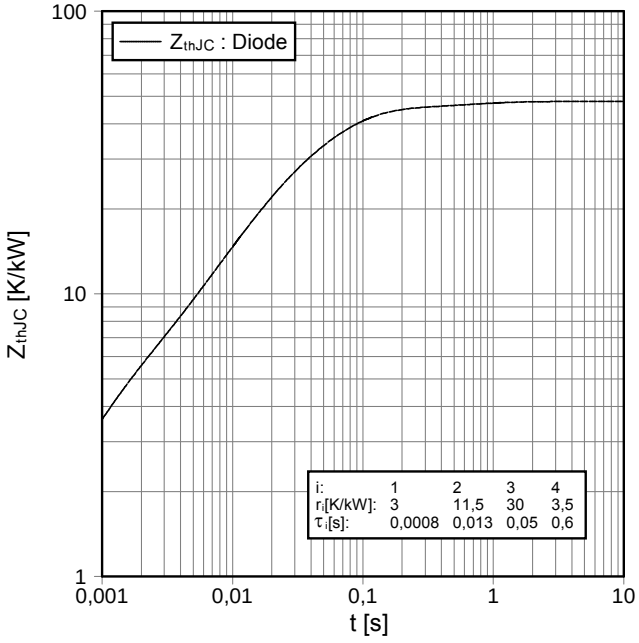

NTC-Temperaturkennlinie (typisch)
NTC-temperature characteristic (typical)
$R = f(T)$

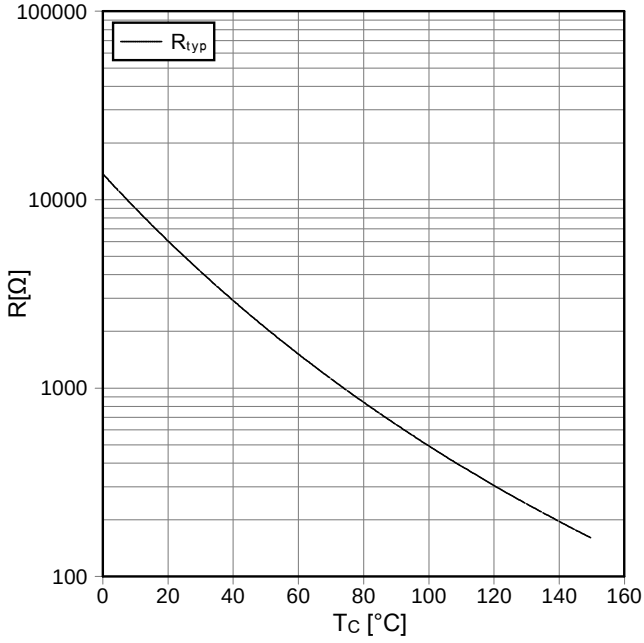

prepared by: RH	date of publication: 2009-08-28
approved by: MS	revision: 3.1

Schaltplan / circuit diagram

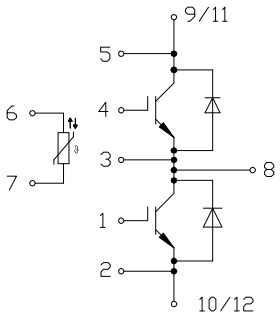

Gehäuseabmessungen / package outlines

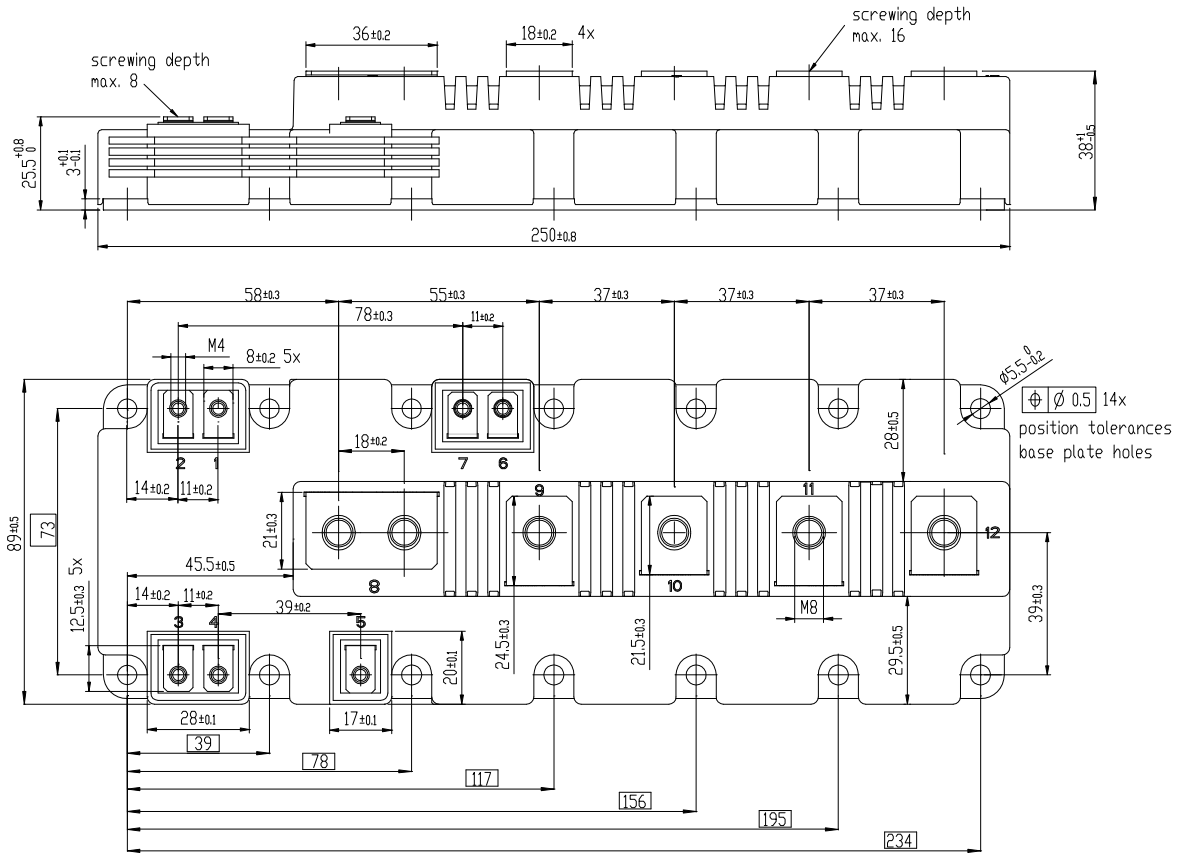

prepared by: RH	date of publication: 2009-08-28
approved by: MS	revision: 3.1

Nutzungsbedingungen

Die in diesem Produktdatenblatt enthaltenen Daten sind ausschließlich für technisch geschultes Fachpersonal bestimmt. Die Beurteilung der Eignung dieses Produktes für Ihre Anwendung sowie die Beurteilung der Vollständigkeit der bereitgestellten Produktdaten für diese Anwendung obliegt Ihnen bzw. Ihren technischen Abteilungen.

In diesem Produktdatenblatt werden diejenigen Merkmale beschrieben, für die wir eine liefervertragliche Gewährleistung übernehmen. Eine solche Gewährleistung richtet sich ausschließlich nach Maßgabe der im jeweiligen Liefervertrag enthaltenen Bestimmungen. Garantien jeglicher Art werden für das Produkt und dessen Eigenschaften keinesfalls übernommen.

Sollten Sie von uns Produktinformationen benötigen, die über den Inhalt dieses Produktdatenblatts hinausgehen und insbesondere eine spezifische Verwendung und den Einsatz dieses Produktes betreffen, setzen Sie sich bitte mit dem für Sie zuständigen Vertriebsbüro in Verbindung (siehe www.infineon.com, Vertrieb&Kontakt). Für Interessenten halten wir Application Notes bereit.

Aufgrund der technischen Anforderungen könnte unser Produkt gesundheitsgefährdende Substanzen enthalten. Bei Rückfragen zu den in diesem Produkt jeweils enthaltenen Substanzen setzen Sie sich bitte ebenfalls mit dem für Sie zuständigen Vertriebsbüro in Verbindung.

Sollten Sie beabsichtigen, das Produkt in Anwendungen der Luftfahrt, in gesundheits- oder lebensgefährdenden oder lebenserhaltenden Anwendungsbereichen einzusetzen, bitten wir um Mitteilung. Wir weisen darauf hin, dass wir für diese Fälle
- **die gemeinsame Durchführung eines Risiko- und Qualitätsassessments;**
- **den Abschluss von speziellen Qualitätssicherungsvereinbarungen;**
- **die gemeinsame Einführung von Maßnahmen zu einer laufenden Produktbeobachtung dringend empfehlen und gegebenenfalls die Belieferung von der Umsetzung solcher Maßnahmen abhängig machen.**

Soweit erforderlich, bitten wir Sie, entsprechende Hinweise an Ihre Kunden zu geben.

Inhaltliche Änderungen dieses Produktdatenblatts bleiben vorbehalten.

Terms & Conditions of usage

The data contained in this product data sheet is exclusively intended for technically trained staff. You and your technical departments will have to evaluate the suitability of the product for the intended application and the completeness of the product data with respect to such application.

This product data sheet is describing the characteristics of this product for which a warranty is granted. Any such warranty is granted exclusively pursuant the terms and conditions of the supply agreement. There will be no guarantee of any kind for the product and its characteristics.

Should you require product information in excess of the data given in this product data sheet or which concerns the specific application of our product, please contact the sales office, which is responsible for you (see www.infineon.com, sales&contact). For those that are specifically interested we may provide application notes.

Due to technical requirements our product may contain dangerous substances. For information on the types in question please contact the sales office, which is responsible for you.

Should you intend to use the Product in aviation applications, in health or live endangering or life support applications, please notify. Please note, that for any such applications we urgently recommend
- **to perform joint Risk and Quality Assessments;**
- **the conclusion of Quality Agreements;**
- **to establish joint measures of an ongoing product survey, and that we may make delivery depended on the realization of any such measures.**

If and to the extent necessary, please forward equivalent notices to your customers.

Changes of this product data sheet are reserved.

prepared by: RH	date of publication: 2009-08-28
approved by: MS	revision: 3.1